

1-1-2008

Selective disruption of hte blood-brain barrier by photochemical internalization

Michelle Jie Zhang
University of Nevada, Las Vegas

Follow this and additional works at: <https://digitalscholarship.unlv.edu/rtds>

Repository Citation

Zhang, Michelle Jie, "Selective disruption of hte blood-brain barrier by photochemical internalization" (2008). *UNLV Retrospective Theses & Dissertations*. 2438.
<http://dx.doi.org/10.25669/kw8o-jher>

This Thesis is protected by copyright and/or related rights. It has been brought to you by Digital Scholarship@UNLV with permission from the rights-holder(s). You are free to use this Thesis in any way that is permitted by the copyright and related rights legislation that applies to your use. For other uses you need to obtain permission from the rights-holder(s) directly, unless additional rights are indicated by a Creative Commons license in the record and/or on the work itself.

This Thesis has been accepted for inclusion in UNLV Retrospective Theses & Dissertations by an authorized administrator of Digital Scholarship@UNLV. For more information, please contact digitalscholarship@unlv.edu.

SELECTIVE DISRUPTION OF THE BLOOD-BRAIN BARRIER
BY PHOTOCHEMICAL INTERNALIZATION

by

Michelle Jie Zhang

Bachelor of Arts
University of Nevada, Las Vegas
2004

A thesis submitted in partial fulfillment
of the requirements for the

Master of Science Degree in Health Physics
Department of Health Physics
School of Allied Health Sciences

Graduate College
University of Nevada, Las Vegas
December 2008

UMI Number: 1463541

INFORMATION TO USERS

The quality of this reproduction is dependent upon the quality of the copy submitted. Broken or indistinct print, colored or poor quality illustrations and photographs, print bleed-through, substandard margins, and improper alignment can adversely affect reproduction.

In the unlikely event that the author did not send a complete manuscript and there are missing pages, these will be noted. Also, if unauthorized copyright material had to be removed, a note will indicate the deletion.

UMI[®]

UMI Microform 1463541

Copyright 2009 by ProQuest LLC.

All rights reserved. This microform edition is protected against unauthorized copying under Title 17, United States Code.

ProQuest LLC
789 E. Eisenhower Parkway
PO Box 1346
Ann Arbor, MI 48106-1346



Thesis Approval
The Graduate College
University of Nevada, Las Vegas

November 6, 20 08

The Thesis prepared by

Michelle Jie Zhang

Entitled

Selective Disruption of the Blood-Brain Barrier by Photochemical
Internalization

is approved in partial fulfillment of the requirements for the degree of

Master of Science in Health Physics

Examination Committee Chair

Dean of the Graduate College

Examination Committee Member

Examination Committee Member

Graduate College Faculty Representative

Examination Committee Member

ABSTRACT

Selective Disruption of the Blood-Brain Barrier by Photochemical Internalization

by

Michelle Jie Zhang

Dr. Steen Madsen, Examination Committee Chair
Associate Professor of Health Physics
University of Nevada, Las Vegas

Failure to eradicate infiltrating glioma cells using conventional treatment regimens results in tumor recurrence and is responsible for the dismal prognosis of patients with glioblastoma multiforme (GBM). This is due to the fact that migrating glioma cells are protected by the blood-brain barrier (BBB) which prevents the delivery of most anti-cancer agents. The overall objective of this work was to evaluate the ability of photochemical internalization (PCI) to selectively disrupt the BBB in rats. This will permit access of anti-cancer drugs to effectively target infiltrating tumor cells, and potentially improve the treatment effectiveness for malignant gliomas.

PCI treatment, coupling the macromolecule *Clostridium perfringens* (*Cl p*) epsilon prototoxin with ALPcS_{2a}-photodynamic therapy (PDT), was performed on non-tumor bearing inbred Fischer rats. T2-weighted and T1-weighted post-contrast magnetic resonance imaging (MRI) scans were used to evaluate the extent of BBB disruption which was inferred from treatment-induced edema and contrast volumes.

The PCI effect in rat brain was found to be dependent on light fluence, photosensitizer concentration, *Cl p* prototoxin concentration and administration route.

Selective disruption of the BBB by PCI was observed for intraperitoneal administration of 1:100 stock dilutions of *Clp* prototoxin and photosensitizer concentrations and light fluences of 1 mg/kg and 1 J respectively. Single modality treatments consisting of PDT or *Clp* resulted in only minimal damage to the BBB.

PCI was found to be highly effective for inducing selective and localized disruption of the BBB. The extent of BBB opening peaked on day 3 and was completely restored by day 18 after PCI.

TABLE OF CONTENTS

ABSTRACT.....	iii
LIST OF FIGURES	vi
ACKNOWLEDGMENTS	vii
CHAPTER 1 INTRODUCTION	1
Malignant Gliomas.....	1
The Blood-Brain Barrier	6
Strategies for Delivering Drugs to the Brain	17
A BBB Opening Agent: Clostridium Perfringens	21
Photodynamic Therapy	27
Photochemical Internalization	39
Proposal and Hypothesis of PCI Study in BBB Disruption.....	42
CHAPTER 2 MATERIALS AND METHODS.....	44
Experimental Animals	44
PDT-only Treatment Protocol.....	44
<i>C/p</i> -only Treatment Protocol	46
PCI Treatment Protocol	46
MR Imaging	47
Data Analysis	48
CHAPTER 3 RESULTS	49
Comparison of Light Delivery Method in AlPcS _{2a} -PDT	49
Comparison of BBB Disruption Induced by ALA-PDT and AlPcS _{2a} -PDT	50
Effects of Photosensitizer Concentration in AlPcS _{2a} -PDT	52
Effects of Light Fluence Level in AlPcS _{2a} -PDT	54
Surviving Fraction of Rats Following <i>C/p</i> Prototoxin Exposure.....	55
BBB Disruption Induced by the PCI Effect.....	56
CHAPTER 4 DISCUSSION	62
CHAPTER 5 CONCLUSIONS.....	68
REFERENCES	70
VITA	75

LIST OF FIGURES

Figure 1	Structure of the Blood-Brain Barrier	8
Figure 2	Structure of the Tight Junctional Complex at the BBB	9
Figure 3	Amino Acid Sequence of <i>Cl p</i> Epsilon Prototoxin and Toxin.....	23
Figure 4	Representations of Photosensitizer Lowest Singlet and Triplet States.....	28
Figure 5	Diagram of the Primary Photophysical Processes of PDT	29
Figure 6	Representation of Oxygen Lowest Singlet and Triplet States	31
Figure 7	Chemical Structures of Porphyrin and Phthalocyanine	34
Figure 8	Chemical Structures of ALA and Its Product PpIX.....	35
Figure 9	Structure of AlPcS _{2a}	36
Figure 10	Illustration of the PCI Mechanism.....	42
Figure 11	Comparison of animal survival after PDT using interstitial or surface irradiation.....	50
Figure 12	Comparison of BBB disruption induced by ALA-PDT and AlPcS _{2a} -PDT .	51
Figure 13	Contrast and edema volumes induced by PDT with varied photosensitizer concentrations	53
Figure 14	Contrast and edema volumes induced by PDT with varied light fluence levels	54
Figure 15	Surviving fraction of animals receiving <i>Cl p</i> prototoxin through different administration routes at varied concentrations	56
Figure 16	Comparison of contrast and edema volumes induced by PDT and PCI at a light fluence of 2.5 J.....	57
Figure 17	Comparison of contrast and edema volumes induced by PDT and PCI (i.p.) at a light fluence of 1 J.....	58
Figure 18	Comparison of T1-weighted post contrast MRI scans after PDT and PCI treatment	59
Figure 19	Comparison of contrast and edema volumes induced by PDT, PCI (i.c.) and PCI (i.p.) at a light fluence of 1 J.....	60
Figure 20	Comparison of contrast and edema volumes induced by PDT and PCI at a light fluence of 0.5 J.....	61

ACKNOWLEDGMENTS

Michelle Zhang is grateful to Dr. Steen Madsen for being a great mentor throughout the years and for many thoughtful suggestions made in this paper, to Dr. Henry Hirschberg for performing all the surgical experiments and for many useful discussions, to Dr. Michael Gach for his support on acquiring MR images, to David Chighvinadze for his experimental and MR imaging help, and to Dr. Phillip Patton, Dr. Ralf Sudowe and Dr. Daniel Young for their participations in reviewing this study.

CHAPTER 1

INTRODUCTION

1.1 Malignant Gliomas

According to the Central Brain Tumor Registry of the United States (CBTRUS) 2005-2006 statistical report, there were 43,800 new adult cases of brain tumors diagnosed in 2005. 20,500 of these cases were malignant with 12,700 deaths estimated in 2007. Gliomas represent 40% of all primary brain tumors, contributing up to 78% of all malignant brain tumor cases. Due to the large number of patients with malignant gliomas and the continued poor prognosis, it is important to study the essential factors that limit the treatment effectiveness for malignant gliomas and evaluate the efficacy of methods that specifically target these factors.

1.1.1 Origin of Gliomas

Gliomas are primary brain tumors that arise from glial cells. The central nervous system (CNS) has four types of glial cells: (1) ependymal cells, which line the cavities of the CNS and make up the walls of the ventricles, with functions related to the cerebrospinal fluid (CSF); (2) astrocytes, the largest and most common of glial cells: the slender cytoplasmic extensions of astrocytes end in “feet” like processes that wrap around capillaries, and chemicals secreted by astrocytes are responsible for maintaining the special permeability characteristics of endothelial cells that line the capillaries; (3) oligodendrocytes, having fewer processes than astrocytes, are responsible for the

myelination of neuronal axons; (4) microglia, or phagocytic cells, the least numerous and smallest glial cells in the CNS. These cells are capable of migrating through neural tissue and act as a janitorial service by swallowing up waste products and pathogens (Martini, 2006).

A glioma either develops from a single type of glial cell such as astrocytes to form astrocytoma, or contains cells from multiple lines of glial cells such as oligoastrocytoma. Since all glial cells are responsible for providing support and nutrients to neurons, maintaining homeostasis, forming myelin, destroying pathogens and dead neurons, and participating in signal transmission in the nervous system, the formation of malignant gliomas in patients seriously damages their quality of life. Since the number of glial cells in the CNS greatly exceeds neurons (by approximately ten times), the probability of glioma formation is relatively high.

1.1.2 Classification of Malignant Gliomas

Based on various histological features accompanied by genetic alterations, malignant gliomas are classified as grade II, III or IV by the World Health Organization (WHO), corresponding to increased tumor aggressiveness. Moderate proliferation and invasion are usually associated with grade II malignant gliomas. Patients diagnosed with grade II gliomas have a survival range of 5-10 years. The degree of tumor cell proliferation and invasion are increased in grade III gliomas, with a median patient survival of 2-3 years. In addition, angiogenesis which refers to a physiological process involving the growth of new blood vessels from pre-existing vessels is initiated at this stage. Angiogenesis increases the aggressiveness of tumor cells by supplying them with more oxygen and nutrients through the newly formed blood vessels. Further differentiation of brain tumor

cells results in grade IV malignant gliomas, which exhibit significant increases in proliferation, invasion, angiogenesis and necrosis. The median survival of patients with grade IV gliomas is 12 months (Furnari et al., 2007).

1.1.3 Invasion Property of Gliomas

The potential clinical benefits of understanding the biological basis of glioma proliferation, invasion, angiogenesis and necrosis cannot be overstated. Although invasion is a common threat in all grades of malignant gliomas, the biological mechanisms involved in this process are not fully understood and continue to be a subject of active study. The most frequent route of invasion of glioma cells occurs along white matter tracts and basement membranes of blood vessels. In addition, glioma cells have also been found to grow around neurons in the gray matter and to spread along the subpial space (Louis, 2006). The subject of ongoing studies is to determine the reasons that favor such preferential infiltration. One possible explanation involves the integrin receptors that are overexpressed in malignant glioma cells. These specific glioma cell surface receptors ($\alpha_2\beta_1$, $\alpha_5\beta_1$, $\alpha_6\beta_1$, $\alpha_v\beta_3$) interact with extracellular matrix molecules tenascin, fibronectin, laminin, and vitronectin, respectively. These result in alterations of the cellular cytoskeleton which is primarily responsible for controlling cell movement. With an altered cytoskeleton, cell locomotion is potentially promoted to yield infiltrated glioma cells. In summary, glioma cell invasion is most likely due to a dynamic interplay between cell-extracellular interactions, cell-cell adhesion, remodeling of the extracellular matrix, and cell motility (Louis, 2006).

1.1.4 Glioblastoma Multiforme

Glioblastoma multiforme (WHO grade IV) is the most common and biologically aggressive malignant glioma. It contributes up to 50% of all malignant gliomas according to the CBTRUS 2005-2006 report data (Chamberlain and Kormanik, 1998). Patient prognosis is poor with median survival approaching 12 months. GBM is composed of poorly differentiated neoplastic cells and characterized by vascular proliferation, necrosis, uncontrolled cellular proliferation and diffuse infiltration. In particular, the diffuse infiltrative nature of GBMs makes them extremely difficult to treat by conventional methods.

1.1.5 Treatments for GBM

Several novel therapeutic strategies for the treatment of GBM have been developed in recent years. Surgery still remains the primary treatment method. The extent of surgical tumor resection is the most important factor determining length of survival. Clinical data has shown that patients with malignant gliomas who undergo a complete tumor resection generally do better than those with partial tumor resection (Liu et al., 2008). Although a number of techniques have been attempted to improve the extent of tumor resection, the overall percentage of patients who are suitable for complete tumor resection is limited by the location of tumors in eloquent regions of the brain. Therefore patients with residual and measurable disease after definitive surgery are not uncommon.

Adjuvant therapies consisting of ionizing radiation and chemotherapy are often prescribed immediately after surgery in order to eliminate residual glioma cells. New techniques in radiotherapy are under active study with the goal of improving therapeutic efficacy while reducing toxicity. For example, accelerated radiotherapy schemes are

actively being investigated. They have the advantage of shortening treatment times and decreasing tumor repopulation with less total radiation dose. Hyperfractionation radiotherapy which seeks to improve treatment efficacy by increasing the total dose of radiation while maintaining the total treatment time is under active study, as is stereotactic radiosurgery, which has the benefit of a high degree of dose conformity to the target volume (Liu et al., 2008). Finally, radiosensitizers have been tried in a number of clinical trials without much success due to toxicity-related complications. Although overall survival rates have not improved significantly with these advances in radiotherapy, quality of life has improved due to a reduction in radiation-induced toxicity.

Notwithstanding the recent discovery of Temozolomide (TMZ), standard chemotherapeutic regimens have been relatively ineffective against malignant gliomas. Recent studies consisting of TMZ and radiation have shown that this treatment regimen may be beneficial for GBM patients, resulting in improved overall survival (OS) and time-to-progression (TTP) (Liu et al., 2008). For example, Stupp et al. (2005) conducted a randomized phase III study of 573 patients with newly diagnosed GBM to receive radiotherapy (60 Gy) plus continuous daily TMZ at 75 mg/m² followed by six cycles of adjuvant TMZ at 150-200 mg/m² days 1-5 every 28 days. The overall survival of patients receiving radiation and TMZ was improved to 14.6 months compared to 12.1 months with radiotherapy (60 Gy) alone. Another randomized phase II study by Athanassiou et al. (2005) involving 130 GBM patients using TMZ and radiation followed by a dose-intense adjuvant schedule of 150 mg/m² on day 1-5 and 15-19 every 28 days, resulted in TTP of 10.8 months compared to 5.2 months and increased 1-year OS of 56.3% compared to 15.7% in patients receiving radiation alone.

Even with substantial improvements in conventional treatments consisting of surgery, radiation therapy and chemotherapy, the prognosis for patients with malignant gliomas has not improved significantly over the past four decades. Although complete removal of the bulk tumor is possible with current available techniques, patients continue to relapse. This is due to the aggressive infiltrating nature of malignant gliomas: many glioma cells have already infiltrated 2-3 cm into the surrounding normal brain at the time of bulk tumor resection. These infiltrative tumor cells are well embedded in brain tissues, supplied with nutrients and oxygen by the normal brain vasculature and consequently, also protected by the blood-brain barrier (BBB) which prevents any harmful substances from entering the brain. Few anti-cancer drugs can effectively cross this barrier to target the infiltrating tumor cells. Failure to eradicate infiltrating glioma cells inevitably results in tumor recurrence and further treatments are usually palliative in scope. Therefore, destruction of infiltrating tumor cells is the most crucial step for curing malignant gliomas. This cannot be accomplished until methods are developed to: (1) deliver drugs across the BBB, or (2) selectively disrupt this protective barrier.

1.2 The Blood-Brain Barrier

Since the neural activity of the central nervous system (CNS) requires precise homeostasis of the neural microenvironment, protection from toxic substances circulating in the bloodstream, and efficient nutrient delivery and waste removal, the BBB has evolved at the critical interfaces where blood comes into contact with neural tissues to create and maintain the optimal environment for the CNS.

The BBB is formed by tightly connected brain capillary endothelial cells (Figure 1). Substantially different than those found in peripheral microvessels, the endothelial cells lining the brain vessels are connected by much tighter junctional complexes to completely seal the paracellular spaces and form a continuous physical barrier between the CNS and blood circulation (Abbott, 2005). Both the lumen-facing (luminal, apical) and the brain-facing (abluminal, basal) membranes of the endothelium are made up of phospholipid bilayers lacking fenestrations. The luminal and abluminal membranes of the capillary endothelium are separated by approximately 200 nm of endothelial cytoplasm (Pardridge, 2005). Molecules crossing the BBB must traverse these two limiting membranes of the endothelium. The brain side of the capillary endothelial cells is completely covered by a basement membrane with the end-foot processes of the astrocytes closely attached to it. Pericytes are embedded in the basement membrane between the endothelial cell and astrocyte process, making particularly close contact with endothelial cells (Abbott, 2005). They are thought to provide structural support to the microvasculature and are important in BBB stability (Ballabh et al., 2004). Both the basement membrane and astrocyte foot processes allow diffusion of molecules (Pardridge, 2005) which are free to diffuse through the brain extravascular space once successfully across the limiting membranes.

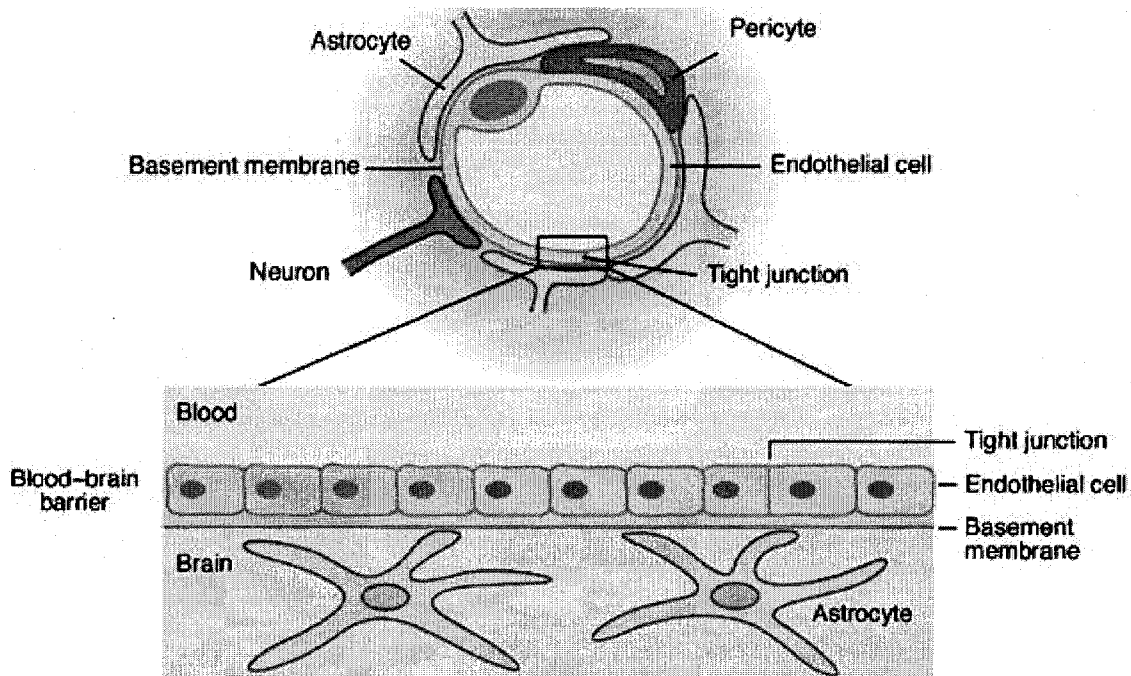


Figure 1. Cross section through a brain microcapillary (upper panel) and the overall structure of the BBB (lower panel). (Modified from: <http://www-ermm.cbcu.cam.ac.uk/03006264h.htm>)

The impermeability of the BBB is the result of a number of unique features of this barrier. Firstly, the physical restriction imposed by tight junctions between endothelial cells greatly reduces paracellular permeability. Additionally, the transport system regulation of endothelial cells limits the number and types of molecules that undergo transcellular transport. Lastly, the metabolic activity of endothelial cells, with powerful enzymes metabolizing many potentially harmful substances, adds to the difficulties faced by molecules trying to penetrate the BBB.

1.2.1 The Physical Barrier: Tight Junctions

The tight junctional complex of the BBB is comprised of a tight junction (TJ) and an adherens junction (AJ). The TJ can be further grouped into three main components:

transmembrane proteins, cytoplasmic accessory proteins, and cytoskeletal proteins (Figure 2).

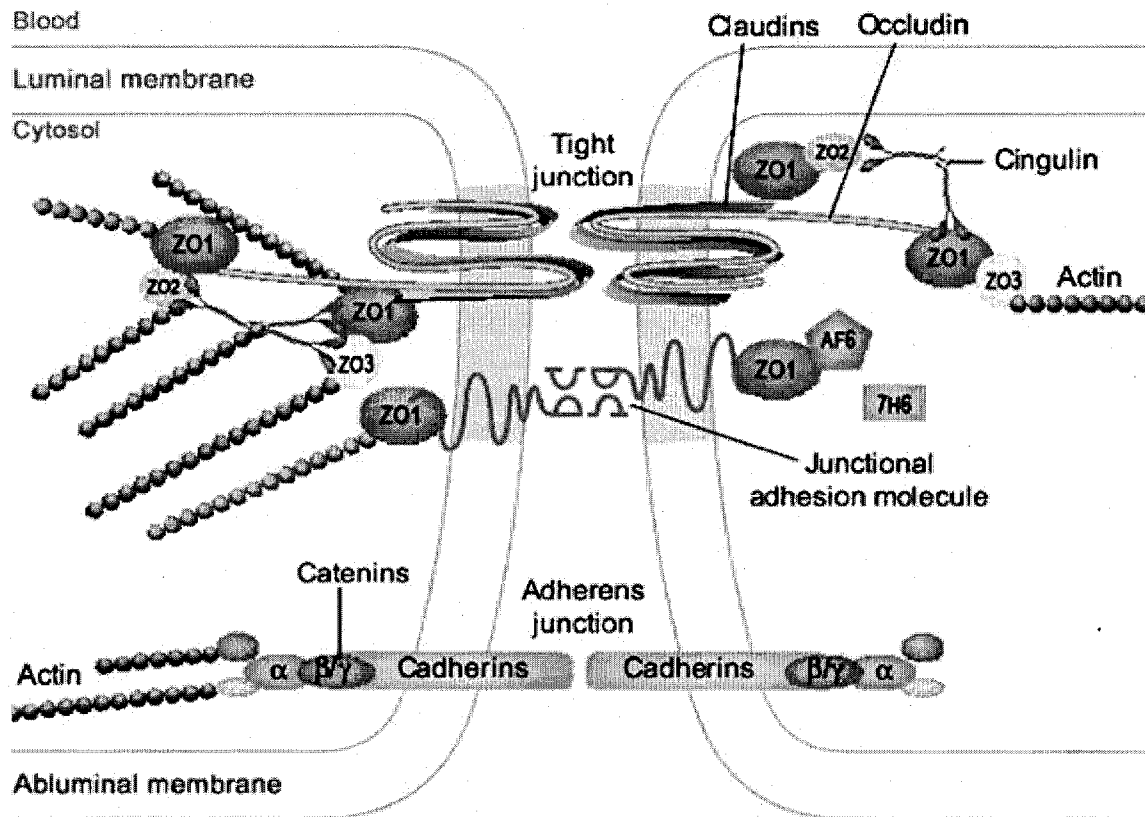


Figure 2. Structure of the tight junctional complex at the BBB. (Modified from ref. Huber et al., 2001)

Three types of transmembrane proteins found at the TJ are occludin, claudins and junction adhesion molecules (JAM). Occludin is a 65 kDa phosphoprotein which was identified as the first transmembrane protein localized at the TJ. It consists of four transmembrane domains, a long COOH-terminal cytoplasmic domain, and a short NH₂-terminal cytoplasmic domain. The two cytoplasmic domains of occludin are responsible for intracellular interaction with the cytoplasmic accessory proteins (Ballabh et al., 2004).

The other two domains of occludin consist of two extracellular loops including about 45 amino acids each (Gloor et al., 2001), which contribute to the regulation of the paracellular barrier of the TJ. It is hypothesized that occludin is needed to regulate rather than establish the properties of the BBB (Wolburg and Lippoldt, 2002). Its presence at the BBB is associated with increased electrical resistance across the barrier and decreased paracellular permeability (Huber et al., 2001).

Claudins, the second type of transmembrane protein of the TJ, are a multi-gene family consisting of at least 24 members that have been identified in both mice and humans. Claudins show an individually restricted expression pattern, suggesting they contribute to tissue-specific properties of TJs (Gloor, 2001). Compared to occludin, claudins are significantly smaller phosphoproteins with a molecular mass of approximately 22 kDa (Ballabh et al., 2004), but they also have four transmembrane domains like occludin, and the COOH-terminal of claudins binds to cytoplasmic accessory proteins. The extracellular loops of claudins bind homotypically to claudins on adjacent endothelial cells to form primary paracellular seals of the TJ (Huber et al., 2001), which indicate the role of claudins for establishing BBB properties.

Together, occludins and claudins form the extracellular component of the TJ and are both required for regulating and establishing the BBB. In the brain, claudin-1, claudin-5 and occludin have been identified in endothelial TJs as required components for the formation of the BBB (Ballabh et al., 2004). Studies have also revealed that the expression of claudin-1, claudin-5 and occludin is reduced in tumor microvessels of GBM (Gloor et al., 2001), which explains the leaky microvasculature associated with GBM.

An additional transmembrane protein, junctional adhesion molecule (JAM), localizing at the TJs belongs to the immunoglobulin (Ig) superfamily. JAM also has a single transmembrane domain and its two extracellular Ig-like loops are formed by disulfide bonds (Ballabh et al., 2004). The overexpression of JAM at the TJs of endothelial cells increases their resistance to chemical diffusion (Gloor et al., 2001). It is therefore suggested that JAM functionally contributes to permeability control of the TJs.

There are a number of cytoplasmic accessory proteins associated with the BBB including the zonula occludens proteins (ZO-1, ZO-2 and ZO-3), cingulin, 7H6 and AF6. ZO-1, ZO-2 and ZO-3 are structurally similar and contain three PDZ domains which help to anchor transmembrane proteins to the cytoskeleton and hold together signaling complexes (Ballabh et al., 2004; Matter and Balda, 2003). These specific domains of ZO proteins facilitate the direct binding to claudins, occludin and JAM. Cingulin interacts with ZO-1, ZO-2, ZO-3, AF6 and others to serve as a scaffolding protein that links cytoplasmic accessory proteins to the cytoskeleton (Huber et al., 2001).

The primary cytoskeletal protein is actin. Actin filaments, the thinnest filaments of the cytoskeleton, are highly versatile. They serve both structural and dynamic roles in the cells (Huber et al., 2001). Actin has known binding sites on all ZO proteins which establish the linkage between the TJ and the cytoskeleton. Studies have also suggested that TJ integrity is dependent on structural organization of actin. An Actin-disrupting substance, such as cytochalasin D, disrupts the structure and function of the TJ.

The adherens junction (AJ) consists of the membrane protein cadherin that joins the actin cytoskeleton via intermediary proteins, catenins, to form adhesive contacts between

endothelial cells. TJ and AJ components are known to interact and influence the tight junctional complex assembly (Ballabh et al., 2004).

Overall, the intrinsic complex structure of the TJs, along with the cytoplasmic accessory proteins linking transmembrane proteins to the actin cytoskeleton, form a continuous precise network of parallel and interconnected strands of proteins and are arranged as a series of multiple barriers to severely restrict the paracellular permeability of the endothelial cells. Therefore, circulating molecules can only gain access to the brain via a transcellular pathway by physically crossing the brain endothelial cells.

1.2.2 Lipid-mediated Diffusion

Since endothelial cell membranes are composed of a lipid bilayer with embedded proteins, some small lipophilic molecules such as O₂ and CO₂ can diffuse freely through the endothelial cells of the BBB and enter the brain. However, most small-molecule drugs that are used today do not cross the BBB effectively. A review of the Comprehensive Medicinal Chemistry (CMC) database shows that, of over 7,000 small-molecule drugs, only 5% demonstrate some effectiveness for a relatively limited number of CNS disorders. The average molecular mass of these CNS active drugs is about 357 Da (Pardridge, 2005).

For a small-molecule drug to cross the BBB in significant amounts, the molecule must have the following two molecular characteristics: 1) molecular mass of less than 400-500 Da and 2) high lipid solubility. For small molecule drugs (< 400 Da) with equivalent molecular mass, drugs with higher lipid solubility generally show increased permeation across the BBB than the ones with lower lipid solubility. However, if the molecular mass of the drug is increased, the permeation of the drug across the BBB will

not increase in proportion to its lipid solubility. For example, experimental data indicates that BBB permeation decreases 100-fold as the molecular mass of the drug is increased from about 200 to 450 Da (Pardridge, 2005). In addition, exponentially decreased BBB permeation is associated with the addition of each pair of hydrogen bonds added to the drug. Once the total number of hydrogen bonds exceeds a threshold value of 8-10, there is only minimal transport of the drug across the BBB in pharmacologically significant amounts (Pardridge, 2005; Scherrmann, 2002). This decrease in permeability is due to the increased likelihood of hydrogen bond formation with water which results in decreased lipid solubility.

Although the increase in lipid solubility of small molecule drugs is likely to increase their penetration through the BBB, it also increases their penetration across all other biological membranes. As the drug is rapidly removed from the blood circulation, the total drug concentration that is encountered at the BBB is substantially decreased. Therefore, the overall drug uptake in the brain is not always increased by increasing drug lipophilicity.

For circulating molecules and therapeutic drugs to cross the BBB by lipid-mediated diffusion, they must be lipid soluble and have a molecular mass less than 400 Da. Furthermore, the fraction of drug bound to plasma proteins must be relatively low and the compound cannot act as a substrate for an active efflux transport system at the BBB (Pardridge, 2005). When molecules fail to satisfy these requirements, the only method for them to cross the BBB is via certain endogenous transport systems localized in the endothelium.

1.2.3 Endogenous Transport Systems

The endogenous transport systems of endothelial cells comprising the BBB can be broadly classified into three categories: 1) carrier-mediated transport (CMT); 2) active efflux transport (AET); and 3) receptor-mediated transport (RMT).

In carrier-mediated transport (CMT), specific carrier proteins localized on the endothelial membrane bind to specific organic molecules or ions and carry them across the membranes. More than 20 carriers have been identified for transporting molecules such as glucose, amino acids, lactic acids and nucleosides into the brain endothelium. Some transporters are located on both the luminal and abluminal membranes of the endothelium, while others are located predominately on one of the two membranes which facilitate the directional transport of the substances (Abbott, 2005). For example, the GLUT-1 transporter which carries the main energy source of the brain (glucose) across the BBB, shows an asymmetrical surface distribution of a 3:1 abluminal:luminal ratio (Dobrogowska and Vorbrodt, 1999). More GLUT-1 glucose transporters localized on the abluminal membrane of the endothelium help to increase the amount of glucose moving in the blood to brain direction, thus supplying the brain with a sufficient energy source.

All forms of CMT across the endothelium have the characteristics of specificity, saturation limits and regulation (Martini, 2006). Each carrier protein in the endothelial membrane will bind and transport only certain substances. For example, the GLUT-1 glucose carrier does not transport other simple sugars while lactic acid is only transported by the MCT-1 carrier. A drug normally not transported across the BBB that is simply coupled with a molecule that crosses the BBB by CMT is unlikely to cross the BBB by this transport system. The rate of transport and the amount of substance that can cross the

BBB by CMT is limited by the availability of carrier proteins. The carriers are said to be saturated when they are operating at maximum speed; the amount of substances crossing the BBB cannot be increased further at the saturation limit.

Active efflux transporters (AET) are capable of transporting solutes out of brain endothelial cells, often with consumption of ATP (Abbott, 2005). P-glycoprotein (Pgp) is a large (140-170 kDa) AET system at the BBB and accounts for the active efflux of molecules in the brain to blood direction (Kemper et al., 2004). It has been established that the Pgp active efflux transporters are present in the luminal membrane of the brain endothelium at high densities. Although some lipophilic drug molecules penetrate the luminal membrane of the brain endothelium, they are then pumped out by the Pgp efflux transporter effectively excluding them from the brain. This efflux activity associated with Pgp transporters explains why some therapeutic drugs show a lower BBB penetration than is predicted from their lipophilicity (Abbott and Romero, 1996). The main function of AET systems similar to Pgp is to restrict a number of potentially harmful substances and lipophilic drugs from entering the brain (Abbott, 2005). One strategy for increasing brain penetration of such drugs is the development of “co-drugs” that inhibit the AET systems at the BBB and thereby allows increased brain penetration of the drugs (Pardridge, 2005).

Large molecules such as peptides and proteins are generally transported across the BBB via the receptor-mediated transport system. In receptor-mediated transport (RMT), the molecule undergoes a specific interaction with a membrane receptor followed by endocytosis to internalize it to the cytoplasm of the endothelium. There are at least three classes of BBB-RMT systems. First, as the name implies, the bidirectional RMT system

causes receptor-mediated transcytosis in both the blood to brain and brain to blood directions. For example, the transferrin receptor (TfR), a bidirectional RMT system, transports transferrin from the blood to brain and transfers apo-transferrin from the brain back to blood. Second, the reverse RMT system, such as the neonatal Fc receptor (FcRn), functions only to mediate the reverse transcytosis in the brain to blood direction. Unlike the first two receptor-mediated transcytosis systems, in the third class of RMT system the receptor-mediated endocytosis mediates the molecule uptake from the blood into the endothelial cell body but this endocytosis is not followed by exocytosis into the interstitial fluid of the brain (Pardridge, 2005). The result of receptor-mediated endocytosis is to internalize the circulating molecules to the endothelial cells of the BBB rather than across the BBB.

In summary, the main feature of the endogenous transport systems of the brain endothelial cells is to limit the transcellular traffic of circulating molecules across the BBB. This is accomplished through: 1) the specificity and saturation limits of carrier-mediated transport; 2) the restriction of potentially harmful substances or lipophilic drug molecules by active efflux transport; and 3) the particularly low rate of receptor-mediated transcytosis or endocytosis.

1.2.4 The Enzymatic Barrier

The endothelial cells of the BBB express a range of Phase I, II and III enzymes. These enzymes are capable of metabolizing many potentially harmful agents (Abbott, 2005), which further restrict the penetration of circulating compounds at the BBB. Several key enzymes in the endothelial cells are capable of breaking down unwanted blood circulating substances and brain metabolites, and thus function as a two-way

metabolic barrier (Abbott and Romero, 1996). In the case of some powerful enzymes, such as monoamine oxidase, their enzymatic activity per gram tissue may approach that of the liver which is the primary organ involved in metabolizing circulating compounds.

In summary, the presence of tight junctions with their complex and interconnected structure prevents paracellular transport of almost all circulating compounds except water molecules. Some small molecules with molecular mass of less than 400 Da and high lipid solubility, may potentially diffuse through the brain endothelial cells. However small-molecule drugs with the appropriate molecular structure and lipophilicity are generally limited by their low therapeutic efficacy for treating CNS diseases, especially malignant gliomas. Multiple endogenous transport systems of the brain endothelium are capable of transporting large molecules, but the specificity of the transporters combined with the low rate of transcytosis/endocytosis greatly restrict the transcellular traffic of these circulating molecules. Additionally, the active efflux transporters and metabolic activity associated with the endothelial cells further restrict potentially harmful substances and lipophilic agents from entering the brain. Taken together, these properties of the brain endothelial cells have made the BBB a serious physical and metabolic barrier which protects the brain from any unwanted substances in the blood plasma. Unfortunately this protective barrier also prevents almost all anti-cancer drugs from crossing the BBB and reaching the infiltrating glioma cells that have migrated from the bulk tumor.

1.3 Strategies for Delivering Drugs to the Brain

Strategies that improve the efficacy of drug delivery to the brain are essential for the successful treatment of a wide variety of CNS disorders including malignant gliomas.

1.3.1 Trans-cranial Drug Delivery

Trans-cranial drug delivery methods that attempt to bypass the BBB include the following three approaches: intracerebral implantation, intracerebroventricular (ICV) infusion, and convection-enhanced delivery (CED) (Pardridge, 2005).

Intracerebral implantations have been tested in patients with malignant brain tumors. These implants consist of polymer wafers loaded with an anti-cancer drug. Following surgical tumor resection, the wafer is placed in the empty surgical cavity and the therapeutic agent (typically BCNU) diffuses through the brain parenchyma. The major limitation of this technique is the limited diffusion capacity of most drugs (Kemper, 2004). This is problematic since malignant glioma cells often migrate several centimeters from the tumor resection region – a distance unlikely to be within the range of the diffusing drug.

Unlike endothelial cells of the BBB, the ependymal cells that line the cavities of the CNS, and the walls of the ventricles, are relatively permeable to molecules circulating in the cerebrospinal fluid (CSF) and the interstitial space of the brain. Therefore, the method of intracerebroventricular (ICV) infusion was developed to take advantage of the increased permeability of the ventricular system. Unfortunately, patients with brain tumors usually do not benefit from ICV drug infusion due to the relatively small surface of the CSF-brain interface and the limited diffusion of most drugs into the brain.

The common factor limiting either intracerebral implantation or the ICV infusion method is the diffusion distance for drug penetration into the brain from the source. Studies have shown that the concentration of drug decreases logarithmically with distance from the source. For example, the concentration of a small molecule decreases

by 90% at a distance of only 0.5 mm from the intracerebral implantation site in rat brain (Pardridge, 2005).

The effective drug diffusion distance in the brain can be increased to a radius of a few millimeters when the drug is delivered through the method of CED. The CED approach delivers therapeutic agents through catheters under continuous positive pressure, either directly into the tumor or through the interstitial space around the resection cavity (Liu et al., 2008). CED used in GBM patients causes a preferential flow of the forced therapeutic agents along the white matter tracts. Unfortunately, this often results in an abnormal increase in the number of astrocytes due to the destruction of nearby neurons along the white matter tracts, and thus raises concerns about the long-term effects of this delivery approach for patients (Pardridge, 2005).

1.3.2 Trans-vascular Drug Delivery

Despite the complex structure and impermeability of the BBB, trans-vascular drug delivery to the brain via endothelial cells of the BBB still represents the main route of drug entry into the CNS. The popularity of trans-vascular over trans-cranial drug delivery is simply due to the favorable biological properties of the brain capillaries.

There are over 100 billion capillaries in the human brain. Since capillaries are separated by approximately 50 μm , the maximum diffusion distance in the brain following trans-vascular delivery is only 25 μm . Even a molecule as large as albumin, with a molecular mass of 68 kDa will diffuse 25 μm in less than 1s (Pardridge, 2005). In comparison, distances between drug sources and infiltrating glioma cells are typically of the order of several cm in the case of intracerebral implants.

The total length of capillaries in the human brain is about 400 miles and the surface area of the brain capillary endothelium is about 20 m² (Pardridge, 2005). The total brain capillary surface area is about 5,000-fold larger than the blood-CSF barrier. The large surface area of the brain capillaries increases the probability of drug penetration and facilitates access of anti-cancer agents to glioma cells due to the relatively short diffusion distances.

Taken together, the relatively short drug diffusion distances and the larger surface area of the brain capillaries are the main advantages of trans-vascular drug delivery through the BBB even though the impermeability of the BBB limits total drug uptake by the brain. Therefore, any chemical agent or method that has the capability of increasing BBB permeability or temporarily disrupting the BBB structure, can rapidly increase the efficiency of drug delivery to the brain through the trans-vascular route.

1.3.3 Disruption of the BBB by Osmotic Opening

Osmotic opening involves the administration of hypertonic solutions to cause shrinkage of the endothelial cells thereby disrupting the tight junctions to enhance the paracellular transport of substances through the BBB. Hypertonic solutions used for this purpose include mannitol, arabinose, saline, and several other agents (Kemper et al., 2004). Mannitol is the most widely investigated agent in BBB disruption. The osmotic opening method has been shown to increase the delivery of chemotherapeutic agents in patients with malignant gliomas, with a subsequent decrease in morbidity and mortality compared with patients receiving systemic chemotherapy alone (Neuwelt et al., 1994). Unfortunately, this method tends to increase the BBB permeability in regions of normal brain as well as the tumor (Abbott and Romero, 1996) which can be problematic since it

facilitates passage of a wide variety of circulating molecules into the brain, thus substantially increasing the risk of neurological effects which may outweigh the benefits of barrier opening.

1.4 A BBB Opening Agent: Clostridium Perfringens

Clostridium perfringens (*Cl p*) is a rod-shaped, gram-positive bacterium measuring approximately $2-4 \times 1-1.5 \mu\text{m}$ (Sakurai, 1995). *Cl p* are classified into four major protein toxins consisting of alpha, beta, epsilon and iota toxins which are produced from a combination of five groups of *Cl p* strains (types A-E). The *Cl p* toxins possess a number of biological activities that may result in necrosis, contraction of smooth muscles, edema and death. In particular, the *Cl p* epsilon toxin and its prototoxin are of interest in this study, since they are known for their ability to cause widespread opening of the BBB.

1.4.1 *Cl p* Epsilon Toxin

Epsilon toxin ($\approx 31.4 \text{ kDa}$), produced by *Cl p* types B and D, is one of the most potent *Cl p* toxins. Administration of this toxin leads to preferential accumulation in the kidneys and in the brain (Soler-Jover et al., 2007). Several studies support the existence of an epsilon toxin receptor in the brain capillary endothelial membrane. Biochemical studies on the binding of *Cl p* epsilon toxin to rat brain membranes indicate a high-affinity binding of the toxin to specific binding sites in brain endothelial membranes. However, the nature of the binding sites on the endothelial membranes is not known (Zhu et al., 2001).

Through binding to specific receptor sites on the brain endothelial membranes, epsilon toxin causes severe damage to the vascular endothelium. The toxin acts very

rapidly and in very small doses to produce a vascular endothelium defect in the brains of mice (Buxton, 1976). The mechanism by which epsilon toxin causes vascular damage is unknown.

Studies of epsilon intoxication in mice brains by light or electron microscopy have revealed some ultrastructural changes in the brain endothelium (Finnie, 1984a; Finnie, 1984b; Morgan and Kelly, 1974; Gardner, 1973). Astrocytes appeared to be particularly sensitive to this toxin as evidenced from ultrastructural findings showing significant astrocyte swelling, especially at the end-feet processes of these cells. These changes were quickly followed by evidence of severe endothelial damage including swelling, loss of cytoplasmic organelles with blebbing of the luminal surface and nuclear pyknosis (Finnie, 2004).

When the epsilon toxin injures the brain capillary endothelium, there is loss of BBB integrity and increased vascular permeability. For example, using horse-radish peroxidase (HRP) as a tracer, it was found that this enzyme can leak from brain blood vessels of mice within 1 h of intravenous toxin administration (Morgan, 1975). Other studies using radioactive tracers have confirmed the ability of epsilon toxin to induce vascular leakage in the mouse brain (Worthington and Mulders, 1975).

The increased vascular permeability of the BBB induced by epsilon toxin leads to a net movement of water, electrolytes and other substances from the blood circulation into the brain parenchyma resulting in severe cerebral edema. In edematous conditions, the astrocytes swell prominently, particularly the processes in close contact with brain capillary endothelial cells (Finnie, 1984a). Diffuse cerebral edema often results in

neurological disorders, such as opisthotonus and convulsions, leading rapidly to death (Dorca-Arévalo et al., 2008).

1.4.2 *Clp* Epsilon Prototoxin

Epsilon toxin is synthesized and secreted as a non-toxic precursor prototoxin that is converted to fully active toxin by proteolytic cleavage. Epsilon prototoxin exists in an inactive form consisting of one polypeptide chain of 311 amino acids with a molecular mass of about 32.7 kDa (Figure 3). Upon exposure to proteolytic enzymes, especially trypsin and chymotrypsin, epsilon prototoxin is activated by cleavage of either amino (NH₂-) or carboxy (COOH-) terminal peptides of 14 and 23 residues respectively to yield the fully activated epsilon toxin (Soler-Jover et al., 2007).

Prototoxin:

5
10
15
20
 Lys-Glu-Ile-(Cys(Cm))-Asx-Pro-Val-Ser-Tyr-Glu-Met-Ser-Tyr-Lys-Ala-Ile-Tyr-Asx-?-Val-

Toxin:

5
10
 Ala-Ile-Tyr-Asx-Asx-Val-Leu-Asx-Pro-Leu-Ile-Glx-

Figure 3. Amino acid sequence of *Clp* epsilon prototoxin and toxin. Amino acids that are not confirmed are in parenthesis and those not identified are labeled with a question mark. (Modified from ref. Bhowan and Habeeb, 1977)

The partial polypeptide chain compositions of epsilon prototoxin and toxin shown in Figure 3 reveal a common sequence of Ala-Ile-Tyr-Asx-Val associated with both molecules. This common sequence starting at the NH₂-terminal end of epsilon toxin is evidence that the process of epsilon prototoxin activation by trypsin involves the scission of one peptide bond between Lys₁₄-Ala₁₅. Therefore, the activation of epsilon prototoxin

to toxin is accompanied by release of a low molecular weight (14 amino acid residues long) peptide from the NH₂-terminal end of prototoxin (Bhown and Habeeb, 1977).

The enzymatic activation increases the toxicity of epsilon toxin at least 1,000-fold over the minimally toxic prototoxin (Finnie, 2004). However, in some cases a longer exposure to proteolytic enzymes may result in further cleavage at newly exposed sites and progressive fragmentation of the biologically active toxin resulting in the loss of toxicity (Bhown and Habeeb, 1977).

The activation of epsilon prototoxin to toxin is associated with only minor conformational changes and is neither accompanied by a large decrease in molecular weight nor by a loss in immunochemical reactivity (Bhown and Habeeb, 1977).

1.4.3 Combined Effects of Epsilon Toxin and Prototoxin

Soler-Jover et al. (2007) used epsilon-toxin-green fluorescence protein (epsilon-toxin-GFP) and epsilon-prototoxin-GFP to track the distribution of epsilon toxin and prototoxin in intravenously administrated mice through direct fluorescence microscopy detection. The results showed that both epsilon-prototoxin-GFP and epsilon-toxin-GFP accumulate on the luminal surface of the vascular endothelium of blood vessels in all areas of the mouse brain. Epsilon-toxin-GFP was also detected in the brain parenchyma surrounding some blood vessels, suggesting that epsilon toxin, but not epsilon prototoxin, has the ability to cross the BBB. Co-injection of epsilon-toxin-GFP with a 10 molar excess amount of epsilon-prototoxin resulted in a reduced distribution or binding of the epsilon-toxin-GFP in the brain, which demonstrates the protective ability of epsilon-prototoxin after co-injection.

The prototoxin, although non-active, binds to the same surface cell receptors as the fully active toxin thus preventing the toxin from binding to the receptor sites and exerting its toxic effects on the brain. However, the biological effects of epsilon toxin are blocked only in the brain, and not other tissues (Finnie, 2004).

The protection of epsilon prototoxin seems to be relatively short lived. Nagahama and Sakurai (1991) concluded that the inhibitory effects of the prototoxin on the immediate lethal activity and binding of the toxin were present for only 10 min after the intravenous injection of the prototoxin in mice. After ten minutes, the prototoxin appeared to have been transported into the cells from the binding sites on the cell surface thus allowing binding of the toxin to the sites again. Buxton (1976) investigated the prototoxin protection time by injecting (i.v.) formalinized epsilon prototoxin at 3, 10, 30, 100 and 750 min prior to the administration of epsilon toxin. The protection of prototoxin was present from 3 min until 100 min, but was less effective by 750 min.

1.4.4 Delayed Effect of Prototoxin on the BBB

An endothelial protein, endothelial barrier antigen (EBA), has been identified as a marker for the BBB in the rat brain. The EBA protein is not expressed by endothelial cells of peripheral organs and tissues, such as the liver, intestine and heart, rather, it appears to be localized exclusively to the luminal membranes of the endothelial cells of the rat brain.

Zhu et al. (2001) conducted a study to test the delayed effects of epsilon prototoxin (via intraperitoneal administration) on the expression of EBA alone without subsequent administration of epsilon toxin. The study showed a reduction in the expression of EBA immunoreactivity in rat brain endothelial cells following in vivo administration of the

inactive epsilon prototoxin. However, the relationship between the reduction in EBA expression and the possible effect of the prototoxin on the brain endothelium is not clear. Results from the study also indicated that animals injected with a higher concentration of the prototoxin showed a faster and stronger response with significant reduction in the expression of EBA immunoreactivity. Data from a group of animals injected (i.p.) with a low concentration of epsilon prototoxin showed mild and late response where the maximum effect was seen quantitatively 7 days post-prototoxin injection. Two animals sacrificed at 12 h and 2 days were not significantly different from the control group, but still showed a trend of reduction in EBA expression. The study also demonstrated that reduction in EBA immunoreactivity was accompanied by mild opening of the BBB to endogenous albumin. A progressive increase in albumin immunoreactivity was noted from 1 to 18 h post-injection. At 24 and 48 h, albumin leakage was at its maximum. At 4 and 7 days, albumin leakage was still present but the intensity of immunoreactivity was reduced significantly.

In summary, *Clp* epsilon toxin causes widespread brain endothelial damage leading to severe disruption of the BBB and cerebral edema. The biological effects of the *Clp* epsilon toxin can be temporarily prevented by prior administration of *Clp* epsilon prototoxin due to competitive binding of receptor sites on the endothelial membranes. Administration of *Clp* epsilon prototoxin alone in the rat model results in a reduction of EBA in brain endothelial cells which is also accompanied by a mild opening of the BBB.

Global opening of the BBB has been observed in response to the administration of osmotic agents or *Clp* toxin and prototoxin. Unfortunately, the severe side effects observed following widespread BBB breakdown outweigh the potential benefits.

Therefore, methods for selective disruption of the BBB allowing targeted drug delivery to the diseased area of the brain are likely to result in greater therapeutic efficacy while minimizing toxicity to normal brain.

1.5 Photodynamic Therapy

Photodynamic therapy (PDT) is a treatment modality combining a photosensitizing drug and light to activate the photosensitizer in an oxygen-dependent manner resulting in oxidation of biomolecules in the light-exposed region. PDT has been approved for the treatment of a variety of conditions including cancer, vascular diseases, viral infections and age-related macular degeneration (Høgset et al., 2004). Recently, there has been a lot of interest in the use of PDT for the treatment of refractory tumors. Due to the fact that PDT does not lead to cumulative toxicity in the patient, and there is no known maximum cumulative dose as exists with both radiation therapy and chemotherapy (Castano, 2005), repeated PDT treatments may be an option over conventional treatment methods. Perhaps more importantly, PDT has a high degree of selectivity for a number of tumors including gliomas.

1.5.1 Photophysics of PDT

A photosensitizer is a drug used in PDT, which upon absorption of light is excited to a physical state that is capable of inducing various reactive oxygen species which, in turn, cause biological damage. The ground state of the photosensitizer has paired electrons with opposite spins in the lowest energy molecular orbital which is known as the singlet state (Figure 4). Upon absorption of a light quantum, an electron is excited to a previously unoccupied orbital of higher energy while maintaining its spin (excited singlet

state). Depending on the amount of energy absorbed, the photosensitizer is excited to the first or higher excited singlet state.

Each excited state consists of a number of vibrational levels with increasing energy (Figure 5). An electron in a high vibrational level of an excited state will rapidly fall to the lowest vibrational level of that excited state. During this process of vibrational relaxation, the energy is dissipated as heat and the photosensitizer drops to its first excited singlet state with a very short lifetime (of the order of nanoseconds).

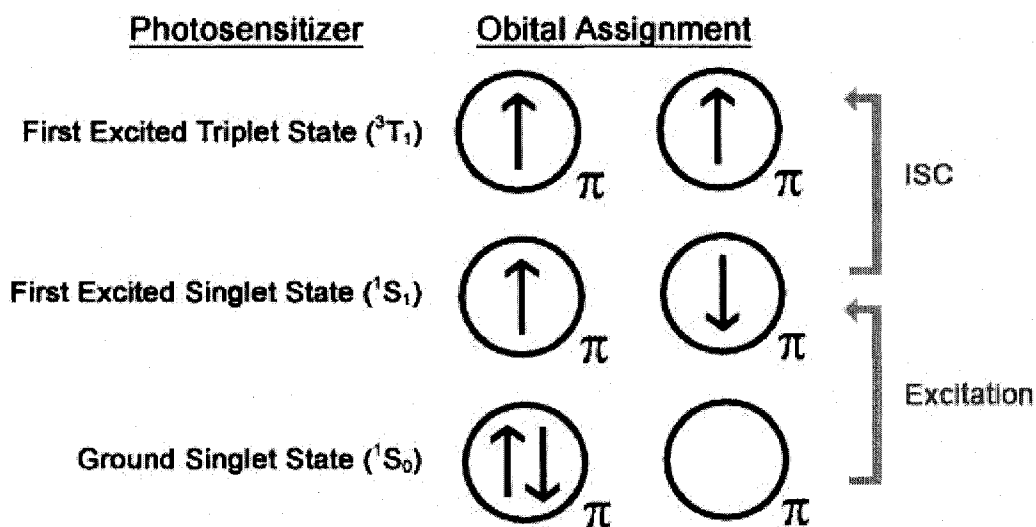


Figure 4. Representations of the lowest singlet and triplet states of a photosensitizer. ISC - intersystem crossing. (Modified from ref. DeRosa and Crutchley, 2002)

The short-lived first excited singlet state can de-excite by emitting a light photon as fluorescence or by internal conversion into heat, returning the photosensitizer to its ground state. The fluorescence emission spectrum of any photosensitizer depends only on its specific electronic structure but not the light wavelength used for excitation. This

fluorescing property of photosensitizers can be used as a diagnostic tool for detecting tumor cells and evaluating the effects of treatment.

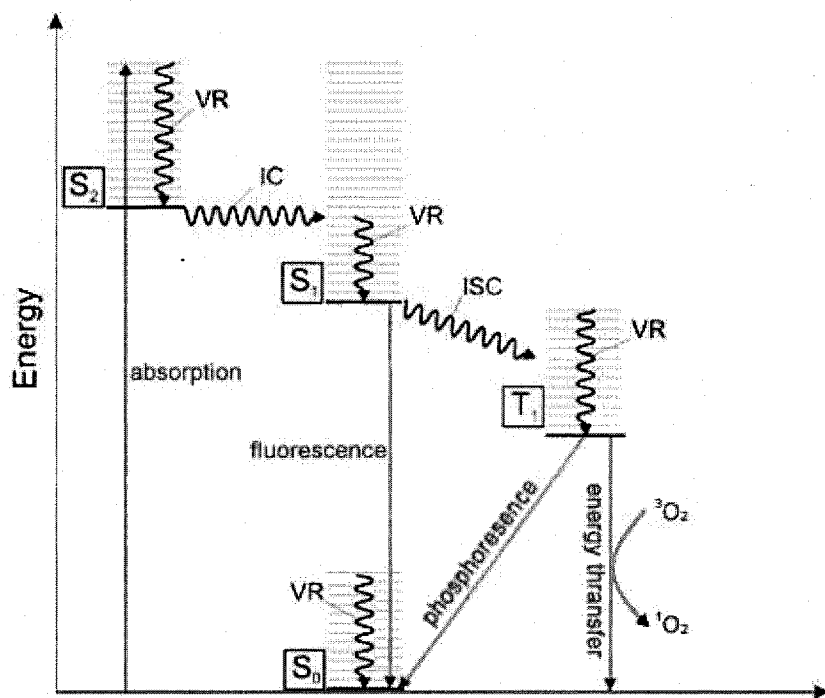


Figure 5. Diagram of the primary photophysical processes of PDT. S_n – singlet states, T_n – triplet states, VR – vibrational relaxation, IC – internal conversion, ISC – intersystem crossing. (Modified from ref. Plaetzer et al., 2008; Calzavara-Pinton et al., 2007)

The first excited singlet state of a photosensitizer having two unpaired electrons with opposite spins may also undergo the process known as intersystem crossing (ISC), where the spin of the excited electron inverts to form the relatively long-lived (microseconds) first excited triplet state that has electrons in a parallel spin configuration. This transition violates the rule of no spin change during a change of an electronic state, however, in the case of macrocyclic molecules with conjugated double bond systems (π -electron system) which are characteristic of most photosensitizers, ISC transitions occur with high

probability. De-excitation of the photosensitizer triplet state directly to its singlet ground state is also a “spin-forbidden” process, the energy loss by emission of light is delayed in this process, known as phosphorescence, and it is also the reason for the relatively long photosensitizer triplet state lifetime (Castano et al., 2004; Castano et al., 2005; Plaetzer et al., 2008).

The most important step of the photophysical processes in PDT is the formation of the triplet state of the photosensitizer. A photosensitizer used in PDT is thus required to have a high quantum yield of triplet state formation. Furthermore, the triplet state must also have a relatively long lifetime for the relevant photochemical reactions to take place.

1.5.2 Photochemistry of PDT

The excited triplet state of a photosensitizer can induce chemical changes in neighboring molecules via two types of mechanisms. Type I mechanisms involve electron or hydrogen atom transfer between the excited photosensitizer and adjacent oxygen molecules or other substrates to produce various reactive oxygen species (ROS). For instance, the formation of superoxide anions (O_2^-) by transfer of an electron from the photosensitizer to an oxygen molecule, is a frequent result of type I reactions. Superoxide can then react to produce another ROS, namely hydrogen peroxide (H_2O_2). At high concentrations, hydrogen peroxide can react with superoxide anions again to form the very reactive hydroxyl radicals ($\cdot OH$). Despite the fact that superoxides are not very reactive in biological systems, further ROS products such as hydrogen peroxide and hydroxyl radicals can easily diffuse through biological membranes and oxidize molecules within a cell to produce cellular damage (Plaetzer et al., 2008).

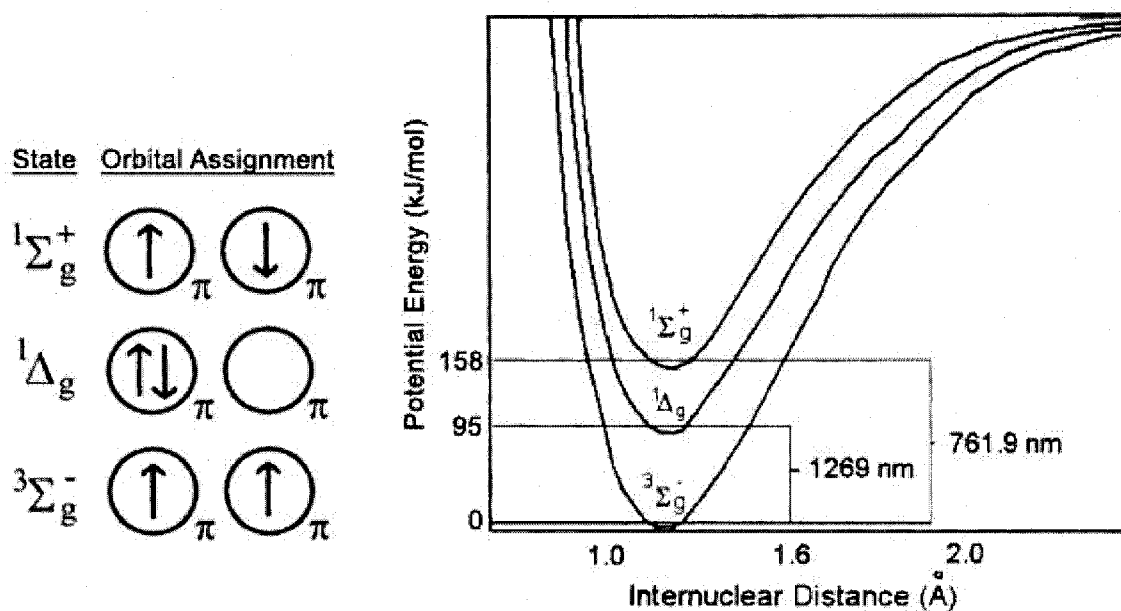


Figure 6. Representation of molecular oxygen's lowest singlet and triplet states and their corresponding potential energy curves. (Modified from ref. DeRosa and Crutchley, 2002)

The type II mechanism involves a direct energy transfer through a collision of the excited photosensitizer with surrounding oxygen molecules to form singlet oxygen - a particularly damaging ROS. As shown in Figure 6, the triplet state configuration ($^3\Sigma_g^-$) represents the ground state of the oxygen molecule which has two unpaired electrons with parallel spins in two different orbitals. The other two configurations of molecular oxygen, $^1\Delta_g$ and $^1\Sigma_g^+$, which represent two forms of excited singlet states are approximately 95 and 158 kJ/mol above the oxygen triplet state, respectively. These potential energies correspond to quantum wavelengths of about 1270 and 762 nm, respectively (DeRosa and Crutchley, 2002). The second excited singlet state of oxygen ($^1\Sigma_g^+$) is short-lived, quickly de-exciting to the first excited singlet state ($^1\Delta_g$). Since the

transition from the $^1\Delta_g$ state to the $^3\Sigma_g^-$ state is spin-forbidden, the oxygen $^1\Delta_g$ state is a relatively long-lived and stable species.

After intersystem crossing, a triplet state of the photosensitizer is formed with an energy of about 110-130 kJ/mol (Plaetzer et al., 2008). Due to the fact that the ground state oxygen molecule exists in a triplet state configuration, it favors the reaction between the triplet state photosensitizer and adjacent oxygen molecules. A minimum energy transfer of about 95 kJ/mol from the triplet state photosensitizer to surrounding oxygen molecule through collision is required to excite the triplet state oxygen to form singlet oxygen. Concurrently, the excited triplet state photosensitizer is converted back to its ground state which is then ready for further cycles of excitation and generation of singlet oxygen. Thus, the triplet state photosensitizer must exceed this energy threshold which equals the potential energy gap of $^1\Delta_g$ state oxygen and the ground state $^3\Sigma_g^-$ (approx. 95 kJ/mol) corresponding to a photon wavelength of 1270 nm.

The singlet oxygen formation ability of a photosensitizer is measured by its quantum yield (Φ_Δ). The quantum yield of singlet oxygen formation of a photosensitizer is commonly determined by detecting the 1270 nm luminescence associated with singlet oxygen relaxation. Almost all photosensitizers used in PDT have a high quantum yield for singlet oxygen formation (approx. 0.3 to 0.5) (DeRosa and Crutchley, 2002).

Singlet oxygen in its excited energy state oxidizes substrates that are normally unaffected by oxygen in its ground state. Its powerful oxidizing ability makes singlet oxygen the primary cytotoxic agent responsible for many photobiological activities. In particular, singlet oxygen causes membrane damage by oxidizing amino acids,

unsaturated fatty acids and cholesterol, which are the primary constituents of biological membranes (Berg et al., 2005).

Since singlet oxygen has a very short lifetime (< 0.1 millisecond) in biological systems, its range of action is confined to approximately 10-20 nm (Castano et al., 2004). Therefore, only molecules and structures that are very close to the area of singlet oxygen production, corresponding to the area of photosensitizer localization, are directly affected by PDT.

It is worthwhile to note that, during the PDT process, photosensitizer molecules can be chemically modified or even degraded by a direct attack of singlet oxygen or other ROS through a process termed photobleaching. Each photosensitizer molecule typically produces 10^3 - 10^5 molecules of singlet oxygen before being degraded through photobleaching by singlet oxygen or by some other process (DeRosa and Crutchley, 2002). Photobleaching is a necessary process in order to clear out the photosensitizer from the biological system in a short period of time.

Both type I and II mechanisms of photochemical reactions in PDT can occur simultaneously, and the ratio between these processes depends on the type of photosensitizer used and the concentrations of adjacent substrates and oxygen molecules. Reactive oxygen species produced from the photochemical reactions, especially singlet oxygen, are powerful oxidizing agents that can directly react with many biological molecules and are thus responsible for all photobiological activities associated with PDT.

1.5.3 Types and Properties of Photosensitizers

Most photosensitizers used in PDT today are porphyrins or porphyrin-related compounds. A structure of the simplest porphyrin is shown in Figure 7a. Porphyrins and

their derivatives have the ability to absorb several wavelengths in the UV-visible region. The long-lived triplet states of many porphyrins allow for high quantum yields of singlet oxygen formation. Some porphyrins undergo rapid degradation in the presence of singlet oxygen (high photobleaching). This could be an advantage in biological systems where rapid breakdown of the photosensitizer is necessary. Porphyrin derivatives also have substituents in the peripheral position of the pyrrole rings and metal ions coordinated at the center which influence their properties including water/lipid solubility, amphiphilicity and stability of the compounds (DeRosa and Crutchley, 2002).

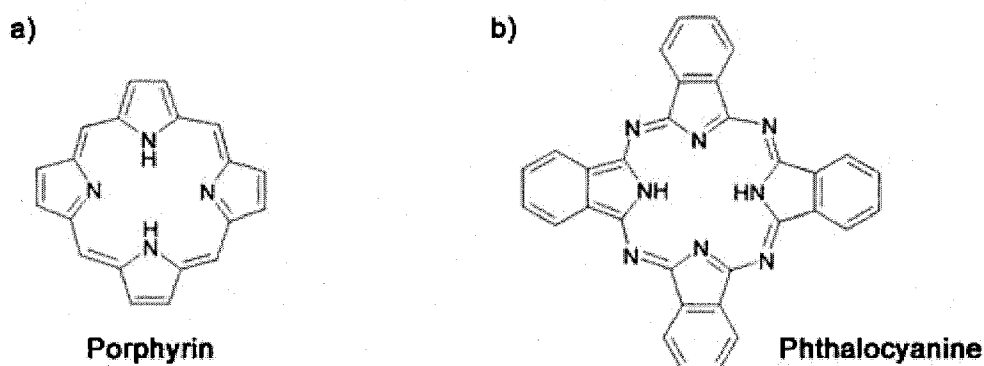


Figure 7. Chemical structures of a) porphyrin and b) phthalocyanine. (Modified from ref. DeRosa and Crutchley, 2002)

The first well-studied porphyrin photosensitizer used in PDT was haematoporphyrin derivative (HpD) or Photofrin II. Despite the high triplet state and singlet oxygen quantum yields of HpD (0.83 and 0.65, respectively) (DeRosa and Crutchley, 2002), it is still far from the ideal photosensitizer. First of all, the complex chemical structure of HpD makes it very difficult to synthesize and purify. Secondly, the absorption of light is weak in the red part of the spectrum where light transmission through tissue is high. Thirdly,

the tumor-to-tissue concentration ratio (selectivity) is poor. Finally, the long-lasting skin photosensitivity of HpD is a clinical disadvantage since patients may have to avoid sunlight for as long as eight weeks (Castano et al., 2004).

In contrast, the use of 5-aminolevulinic acid (ALA) which interacts with the intrinsic cellular heme biosynthetic pathway to produce the photosensitizer, protoporphyrin IX (PpIX) (Figure 8), has attracted great attention due to the short photosensitivity period after application of ALA. ALA is hydrophilic and is taken up mainly by active transport mechanisms in mammalian cells (Calzavara-Pinton et al., 2007). The endogenously formed photosensitizer PpIX is remarkably sensitive to photobleaching and skin photosensitivity lasts for only 1-2 days (DeRosa and Crutchley, 2002). Tumor-to-tissue ratios for ALA-induced PpIX are typically around 10:1 (Berg et al., 2005) compared to 2-3:1 for chemically synthesized photosensitizers.

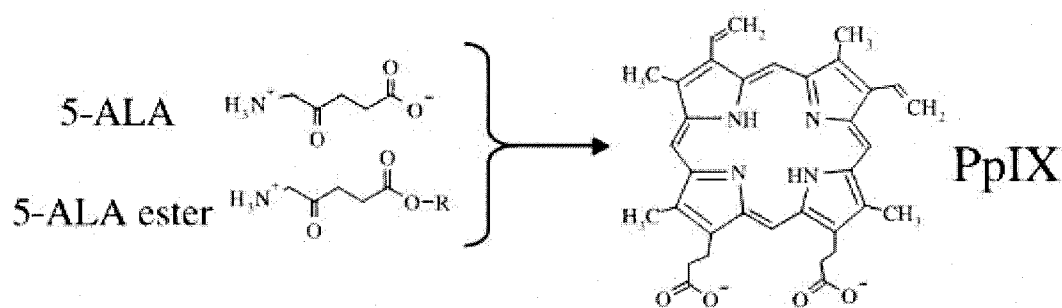


Figure 8. Chemical structures of 5-ALA and its product PpIX. (Modified from ref. Berg et al., 2005)

A second widely studied group of photosensitizers is the phthalocyanines (Pc). The phthalocyanine skeleton (Figure 7b) resembles that of porphyrins (Figure 7a) but an extra aromatic ring is introduced on each pyrrole group which is also linked by nitrogen atoms

instead of the methane carbons in the porphyrins (Berg et al., 1989). The extended conjugation of the peripheral benzene rings in the phthalocyanine structure significantly increases its absorption in the red region of the spectrum (650-700 nm). This absorption spectrum overlaps with the region of maximum light penetration in tissues, thus potentially improving the treatment depths of PDT.



Figure 9. Structure of the photosensitizer aluminum phthalocyanine disulfonate (AlPcS_{2a}). (Modified from ref. Berg et al., 2005)

The photosensitizer, aluminum phthalocyanine disulfonate (AlPcS_{2a}), is a phthalocyanine derivative containing two charged sulfonate groups linked to phthalic subunits in adjacent positions on the Pc molecule and an Al metal ion coordinated at its center (Figure 9). The most important and distinguishable property of AlPcS_{2a} is its amphiphilicity which refers to a chemical compound possessing both hydrophilic and lipophilic properties. Most phthalocyanine photosensitizers are lipophilic and therefore insoluble in water, which makes them unsuitable for use in biological systems. This problem has been solved by sulfonation and by hydroxylation of the benzene rings in the phthalocyanine (Berg et al., 1989). For example, while the phthalocyanine skeleton of

AlPcS_{2a} is lipophilic, the two adjacent sulfonate groups attached to the phthalocyanine molecule contributes to its hydrophilic nature. This amphiphilic photosensitizer is perfectly designed to localize in the cellular membrane (Maman et al., 1999). This is achieved by inserting the lipophilic phthalocyanine skeleton of AlPcS_{2a} in the lipophilic interior of the cellular membrane and dissolving the sulfonate groups in the hydrophilic outer layer of the membrane. AlPcS_{2a} molecules first localize in the cell membrane. During endocytosis, a partial cell membrane with previously localized AlPcS_{2a} molecules pinches inward to form an endocytic vesicle and subsequently, the attached AlPcS_{2a} molecules are transported into the cell via the membrane of the vesicle.

Depending on the physicochemical properties of photosensitizers, they can be taken up by the cell body by endocytosis or by active or passive transport through the plasma membrane. Different photosensitizers will localize differently inside the cell. Since the photosensitizer-generated singlet oxygen has a very short active range in the biological system, the overall biological damage induced by PDT is closely related to the precise subcellular localization of the photosensitizer.

In summary, an ideal PDT photosensitizer should exhibit the following properties: 1) strong light absorption in the red or near infra-red part of the spectrum in order to achieve optimal tissue penetration and minimize the photosensitizer dose required to achieve the desired effect; 2) high triplet state quantum yield ($\Phi_T > 0.4$) and long triplet state lifetime (>1 microsecond); 3) high photostability; 4) amphiphilicity; 5) favorable pharmacokinetics, preferably accumulating rapidly and preferentially in diseased tissues; 6) low levels of dark toxicity and 7) minimal side effects and rapid clearance from the body after PDT (Castano et al., 2004; Castano et al., 2005; Plautner et al., 2008).

1.5.4 PDT Light Dosimetry

Light propagation in biological tissues depends on the following four processes: refraction, reflection, scattering and absorption. Both refraction and reflection are related to the incident angles and can be minimized by applying the light beam perpendicular to the interface between the two media. The scattering of light in tissue has the most pronounced effect on the intensity and directionality of the light beam. Together, refraction and scattering are the primary causes of light attenuation in biological tissues. For PDT on solid tumors, the effective light penetration depth is defined by the depth where light intensity is reduced to 37% of its initial value. For clinical treatments with Photofrin at 630 nm, the light penetration depth is approximately 3-5 mm depending on the tissue (Plaetzer et al., 2008).

1.5.5 Limitations and Advantages of PDT

Although the poor penetration of light through tissues limits PDT treatment volumes, the use of optical fibers for interstitial light delivery, has significantly increased the number of sites accessible to PDT. Even so, the poor penetration depth of red light is a limiting factor for the depth of tumor necrosis achievable in a reasonable time period (Prasmickaite et al., 2002).

The biggest advantage of PDT is dual selectivity (DeRosa and Crutchley, 2002). Firstly, the photosensitizer preferentially localizes in the target tissue. Secondly, the selective light illumination in the target region further confines the photochemical damage. PDT as a new cancer treatment tool thus allows for the possibility of tumor destruction with minimal effects on normal tissues through careful selection of photosensitizers with high tumor specificity. Such specificity is important in a number of

applications including PDT-induced BBB disruption which may be a useful approach for delivering drugs to brain lesions protected by the BBB.

1.6 Photochemical Internalization

Photochemical internalization (PCI) is a novel technology that is under development for utilizing the properties of PDT to enhance the drug delivery of macromolecules in a site-specific manner.

1.6.1 Limitation of Macromolecule Therapy

Although a number of small molecule drugs can readily enter cells, they have relatively low therapeutic specificity primarily due to their structural limitations. In contrast, large macromolecular drugs can easily be coupled to targeting ligands which are able to bind to specific receptors on target cells, thus they have the potential advantage of exerting a higher therapeutic specificity than small molecule drugs.

Since macromolecules are taken up by the cell body through endocytosis, they have to penetrate through the membranes of endocytic vesicles and into the cytosol in order to exert their full biological effects on the cell. Unfortunately, macromolecules generally do not escape easily from endocytic vesicles and consequently, trapped macromolecules are degraded by powerful lysosomal enzymes thereby losing their therapeutic effects. This major limitation of macromolecule therapy has greatly hindered the therapeutic potential of macromolecular drugs (Berg et al., 2006).

In order to improve the drug delivery of macromolecules and exploit their full therapeutic effects, a new technology (PCI) has been introduced which utilizes PDT and

specially designed membrane localizing photosensitizers to target the membranes of endocytic vesicles.

1.6.2 Specific Photosensitizers in PCI

Since the main target of PCI is the membranes of endocytic vesicles, the choice of membrane-localizing photosensitizer is important for effective PCI. In this respect, photosensitizers with an amphiphilic structure are the most efficient since the hydrophilic part of the photosensitizer prevents penetration through the cellular membrane. Once the photosensitizer is securely localized in the cell membrane, it will eventually be incorporated into the membranes of endocytic vesicles via the process of endocytosis. The photosensitizer must maintain its position within the endocytic vesicle while the macromolecular drugs are trapped within the vesicle in order to avoid photochemical destruction of the macromolecules.

AlPcS_{2a} is currently the most popular and preferred photosensitizer for PCI. As detailed in section 1.5.3, AlPcS_{2a} is mainly localized in the membrane of endocytic vesicles. Interestingly, the sulfonation state of AlPcS_n (n=1, 2, 3, 4) is important since different states exhibit different properties. For example, Paquette et al. (1988) have shown that cellular photosensitivity increases with decreasing AlPcS_n sulfonation. This is due to differences in the amount of photosensitizer taken up by the cells: decreasing sulfonation is associated with increasing lipophilicity. The biological activity of these photosensitizers is increased by an order of magnitude as the number of sulfonation groups decreases from 4 to 2 (DeRosa and Crutchley, 2002). Not all sulfonated aluminum phthalocyanines are preferentially localized in the vesicular membranes. For example, tetrasulphonated phthalocyanine is mainly located in the matrix of the endocytic vesicles

(Berg et al., 2006). Therefore, the purity of AlPcS_{2a} used in PCI can directly influence the efficiency and outcome of the PCI method.

1.6.3 Mechanisms of PCI

While specific amphiphilic photosensitizers (e.g. AlPcS_{2a}) preferentially accumulate in the membranes of endocytic vesicles, upon light exposure the photosensitizer interacts with ambient oxygen to produce singlet oxygen. Since singlet oxygen has a very short range of action (< 20 nm), only the area of the vesicular membrane where the photosensitizer is localized will be damaged by singlet oxygen-mediated reactions with amino acids, unsaturated fatty acids and cholesterol in the membrane bilayer. Although the exact structure of the damaged vesicles has not yet been elucidated, the results of vesicular membrane damage (either increased permeability or destructive opening depending on the light fluence and photosensitizer concentration) are easily demonstrated. The previously trapped macromolecular drugs can now be released from the endocytic vesicles into the cytosol in a fully functional form and are free to diffuse to their intended targets (e.g. DNA) to exert their therapeutic effects. The PCI concept is illustrated in Figure 10.

1.6.4 Advantages of PCI

PCI as a drug delivery technology has many advantages. 1) There are no restrictions on the size of the molecules that can be effectively delivered, making PCI highly suitable for a wide variety of molecules. 2) PCI also exhibits high site-specificity, which limits the biological effect to only illuminated areas and lowers the potential systemic side effects of the delivered drug. 3) PCI is a method that increases the therapeutic efficacy of a wide range of macromolecules allowing for the possibility of using lower drug doses to

minimize morbidity. 4) PCI is well suited for combination with other modalities or strategies for targeted drug delivery, thus increasing the potential for further therapeutic improvements (Høgset et al., 2004).

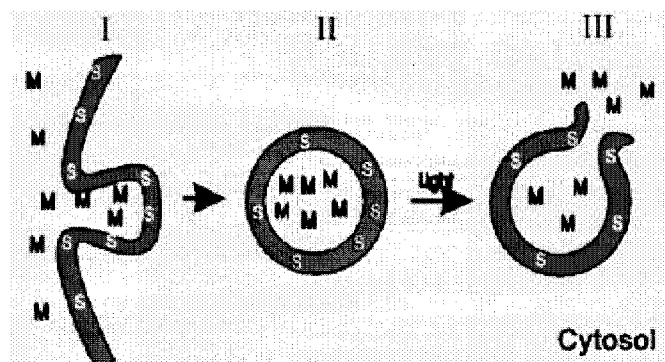


Figure 10. Illustration of the PCI mechanism. M – macromolecule, S – photosensitizer.

(Modified from ref. Høgset et al., 2004)

1.7 Proposal and Hypothesis of PCI Study in BBB Disruption

The efficacy of PCI-mediated delivery of *Clp* epsilon prototoxin for selective opening of the BBB in inbred Fischer rats will be investigated in this study. Since the overall objective of the proposed work is to use PCI to produce localized opening of the BBB, only low concentrations of *Clp* will be administered, i.e., concentrations sufficiently below the threshold for BBB opening. Disruption of the BBB will be achieved by combining sub-threshold doses of *Clp* with sub-threshold PDT light fluences, i.e., the so-called PCI effect. Magnetic resonance imaging will be used to infer the extent of BBB disruption and to track BBB dynamics following each treatment procedure. Specifically, edema formation and gadolinium contrast enhancement will be used as markers for BBB disruption.

It is hypothesized that the biological effects of the *Clp* epsilon prototoxin on the BBB will be potentiated by PCI, but only in areas of the brain exposed to adequate light fluences. Due to this potentiation effect, sub-threshold *Clp* doses will be sufficient to open the BBB. It is hypothesized that the low prototoxin dose will be inadequate to open the BBB in regions where the light fluence is insufficient to evoke the PCI effect.

CHAPTER 2

MATERIALS AND METHODS

2.1 Experimental Animals

Inbred male Fischer rats (Simonsen Laboratories, Inc, Gilroy, CA) weighing about 350 g were used in this study. The animals were housed in the UNLV Animal Care Facility. Animal holding rooms were maintained at constant temperature and humidity on a 12-hour light and dark schedule at an air exchange rate of 18 changes per hour. The animal care and protocol were in accordance with institutional guidelines. All surgical procedures were performed in this facility. For the surgical procedures, the animals were anaesthetized with Pentobarbital (25 mg/kg i.p.). Buprenorphin (0.08 mg/kg s.c.) as a post-operative analgesic was administered to animals following surgery and twice per day for three days thereafter. All animals were euthanized at the end of the study or at the first signs of distress. The euthanasia procedure was accomplished with an overdose of Pentobarbital (100 mg/kg i.p.). In this study, animals were subjected to one of three treatments: (1) PDT-only, (2) *Clp*-only, or (3) PCI.

2.2 PDT-only Treatment Protocol

The photosensitizer, aluminum phthalocyanine disulphonate (AlPcS_{2a}), was diluted to 1.25 mg/ml in PBS and administered (i.p.) 48 hours prior to light treatment. Animals received photosensitizer concentrations of 10, 5 or 1 mg/kg. At the time of the surgical

procedure, each animal was anesthetized with Pentobarbital and fixed in a stereotactic frame. A skin incision was made to expose the skull and a burr hole was made manually with a small gauge needle 1 mm posterior to the bregma and 3 mm to the right of the midline. A 400 μm bare flat-end quartz fiber connected to a portable diode laser was introduced directly into the rat brain to a depth of 5 mm below the dura. Light from the 670 nm diode laser was delivered at a fluence rate of 10 mW. Light fluences of 1, 2, 4, 9 or 26 J were investigated. Treatment times ranged from 100 s to 43 min. After treatment was completed the optical fiber was removed and closure was done with bone wax and sutures.

The interstitial light delivery approach described above resulted in extensive damage to the brain and subsequently a number of animals died soon after treatment, even with the smallest photosensitizer/light dose combination of 1 mg/kg and 1 J. To decrease treatment related morbidity and mortality, surface irradiation was used throughout the remaining light treatments. In this method, most of the PDT treatment procedure remained the same except that no burr hole was drilled. Instead, a skin incision was made exposing the skull and the optical fiber was placed in contact with the surface of the skull at the identical coordinates used to drill the hole for the interstitial treatments. An ALPcS_{2a} concentration of 1 mg/kg combined with light fluence levels of 2.5, 1 or 0.5 J were examined for evaluating the extent of BBB disruption in the group of animals receiving PDT-only treatment.

2.3 *Cl p*-only Treatment Protocol

Cl p epsilon prototoxin stock solution (1 mg/ml) was diluted to three different concentrations of 1:10, 1:50 and 1:100 in PBS. Each concentration was administered (0.7 ml, i.p.) into animals for a toxicity study of *Cl p* epsilon prototoxin.

In addition, a method of intracranial delivery of *Cl p* prototoxin was performed for toxicity comparison. The animal was first sedated and placed in a stereotactic frame. Following skin incision, a small hole was made as previously described and *Cl p* prototoxin (5 µl) was delivered intracranially (1.5 mm below the dura) at a speed of 5 µl/min using a high precision automatic injector (Harvard Apparatus, Cambridge MA). Two different *Cl p* concentrations were investigated: 1:50 and 1:10. The toxicity and the extent of BBB disruption induced by different concentrations of *Cl p* prototoxin with both intraperitoneal and intracranial delivery methods were evaluated.

2.4 PCI Treatment Protocol

Based on individual evaluation of PDT-only and *Cl p*-only treatments, a photosensitizer concentration of 1 mg/kg AlPcS_{2a} was used in the PCI treatments. Three light fluences (2.5, 1 and 0.5 J) were evaluated and both *Cl p* prototoxin delivery methods (i.p.: 1:100 and i.c.: 1:50) were examined.

In a complete PCI treatment procedure, the animal was first injected with photosensitizer AlPcS_{2a} (1 mg/kg, i.p.). 48 hr later, *Cl p* prototoxin was administered either intraperitoneally or intracranially at a concentration described previously. A surface light irradiation was given approximately 60 minutes after *Cl p* administration by

using one of the light fluences determined earlier. The extent of BBB disruption by the PCI effect was evaluated and compared with PDT-only and *C/p*-only treatments.

2.5 MR Imaging

Treated animals were imaged in a 7.0 T animal MR scanner (Bruker) at the Nevada Cancer Institute. Scans were typically acquired on days 1, 3, 5, 8 and 18 post treatments. At the beginning of each imaging session, the animal was anesthetized in an induction chamber connected to isoflurane gas anesthesia. After sedation, the rat was quickly set up on the animal bed of the MR scanner, which was also equipped with a nosecone and tooth-bar fixation system for constant anesthesia throughout the scan. A small surface coil was placed on top of the target area and a T2-weighted (TR = 4200 ms; TE= 36 ms) MR image was acquired. The rat was then removed from the scanner and administered a Gadolinium-based contrast agent (Multihance, 0.8 ml i.p.). A T1-weighted (TR = 700 ms; TE = 14 ms) post contrast MR image was taken 15 – 20 min after the contrast injection.

T2-weighted MR images were used for evaluating the brain edema, which is an indirect result of BBB disruption, induced by PDT-only, *C/p*-only or PCI treatments. Since water molecules have a long T2 relaxation time, which induces a very high T2 signal, edema appears bright on T2-weighted images and is therefore easily visualized.

The gadolinium-based contrast agent (Multihance) has paramagnetic properties, and therefore develops a magnetic moment when placed in a magnetic field. A large local magnetic field produced by this paramagnetic contrast agent can enhance the relaxation rates of water protons in its vicinity (reduce the T1 relaxation time), leading to an increase in signal intensity. That is the reason that Gd-based contrast agents appear bright

on T1-weighted images. Since Multihance, with a molecular weight of 1058.2 Da, is too large to cross the intact BBB, any contrast enhancement evident on T1-weighted images was taken as direct evidence of BBB disruption induced by the corresponding treatment.

2.6 Data Analysis

The extent of BBB disruption from each treatment was evaluated from the degree of contrast enhancement observed on T1 post contrast images and from the edema volume evident on T2 images. The qualitative analyses of contrast and edema volumes were examined using MIPAV (Medical Image Processing, Analysis & Visualization) software. Both contrast and edema volumes were first manually contoured on each T1 or T2 image slice. Then the total volume was calculated automatically by the software according to the following equation: $V = \sum_i (S_i * T) cm^3$ where S_i represents the contrast area contoured on each slice and T represents the image slice thickness (T = 1.0 mm was used in all MR images acquired in this study).

CHAPTER 3

RESULTS

3.1 Comparison of Light Delivery Methods in AlPcS_{2a}-PDT

Both interstitial and surface irradiation methods were evaluated in the PDT-only group of animals. Different concentrations of AlPcS_{2a} combined with varying levels of light fluences were tested under both of the light delivery methods and the results are summarized in Figure 11. The top seven data bars in Figure 11 display the survival time of animals that received interstitial light irradiation. By decreasing the concentration of AlPcS_{2a} from 10 to 1 mg/kg and lowering the light fluence from 26 to 1 J, survival time after PDT treatment was increased from about 20 min at the highest level of the photosensitizer concentration and light fluence combination to about 24 h for the minimum photosensitizer and light fluence combination. In contrast, all animals receiving surface irradiation survived the treatment. In this study, animals that survived for at least 20 days were considered long term survivors. Long-term survival following surface irradiation was observed for all AlPcS_{2a} concentration (1 to 5 mg/kg) and light fluence combinations (2.5, 2, 1, and 0.5 J) investigated in this study.

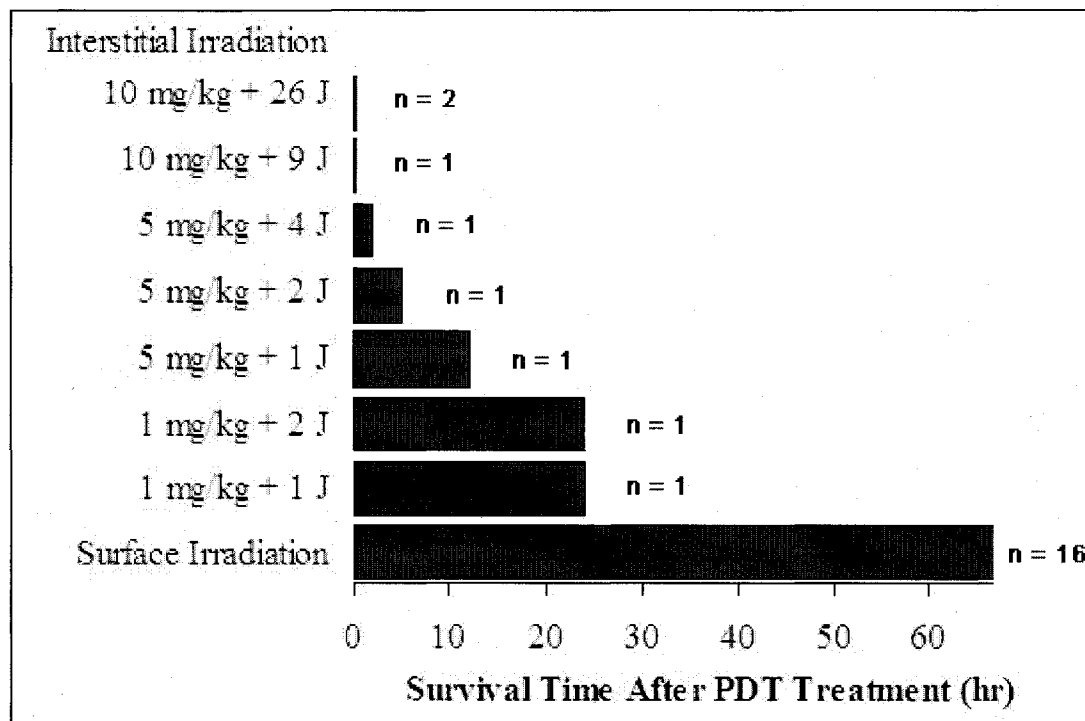


Figure 11. Comparison of animal survival after PDT using interstitial or surface irradiation. The n values to the right of each data bar indicate the number of animals used per group. The top seven data bars represent interstitial irradiation. The surface irradiation data bar represents long-term survival of animals (n = 16) exposed to all photosensitizer and light fluence combinations, including 5 mg/kg + 1 J, 1 mg/kg + 2.5 J, 1 mg/kg + 1 J and 1 mg/kg + 0.5 J.

3.2 Comparison of BBB Disruption Induced by ALA-PDT and AlPcS_{2a}-PDT

In a previous study, PDT treatment with a prodrug (ALA) was evaluated for inducing BBB disruption (Hirschberg et al., 2008). A direct comparison of the extent of BBB disruption between ALA-mediated and AlPcS_{2a}-mediated PDT treatments is shown in Figure 12. Both of the animals were treated using interstitial light delivery. One animal was administrated 125 mg/kg (i.p.) ALA and received a light fluence of 17 J. The result

of T1 post contrast MR images after ALA-PDT treatment shows only a small localized region of contrast enhancement which indicates a minimum amount of BBB disruption (Figure 12 a). In contrast, the animal in scan b) received only 1 mg/kg (i.p.) AlPcS_{2a} and was irradiated to a light fluence of 1 J. With substantially less photosensitizer and a lower light fluence, the T1 post contrast image shown in Figure 12 b suggests a massive BBB disruption following PDT. This extensive BBB disruption explains the reason for the low animal survival associated with interstitial irradiation delivery.

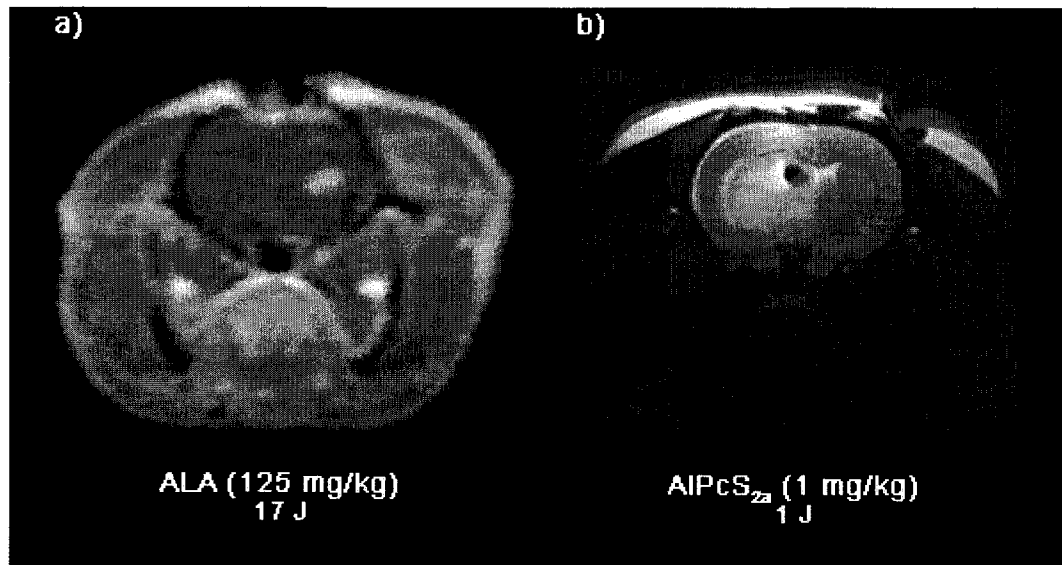


Figure 12. Comparison of BBB disruption induced by ALA-PDT and AlPcS_{2a}-PDT. T1-weighted post contrast MRI scans of rat brains were taken 1 day after PDT treatments. a) ALA-PDT treatment with 125 mg/kg ALA (i.p.) and a light fluence of 17 J (modified from ref. Hirschberg et al., 2008). The image was acquired using a 3 T human scanner. b) AlPcS_{2a}-PDT treatment with 1 mg/kg AlPcS_{2a} (i.p.) and a light fluence of 1 J. The image was acquired using a 7 T small bore animal scanner.

3.3 Effects of Photosensitizer Concentration in AlPcS_{2a}-PDT

Two different AlPcS_{2a} photosensitizer concentrations (5 and 1 mg/kg) were administrated i.p. to two sets of animals 48 h prior to light treatment. A light fluence of 1 J was delivered via surface irradiation to both sets of animals. T2-weighted followed by T1-weighted post contrast MRI scans were taken for each animal on days 1, 3, and 8 after PDT treatment. Both contrast and edema volumes appeared on T1 post contrast and T2 images, respectively, and were calculated separately as shown in Figures 13 a and b.

As illustrated in Figures 13 a and b, there are significant decreases in both edema and contrast volumes with decreasing photosensitizer concentrations indicating that the lower concentration resulted in a reduced degree of BBB disruption following PDT. The data also show a significant reduction in both edema and contrast volumes 8 days following treatment suggesting a gradual closing of the BBB.

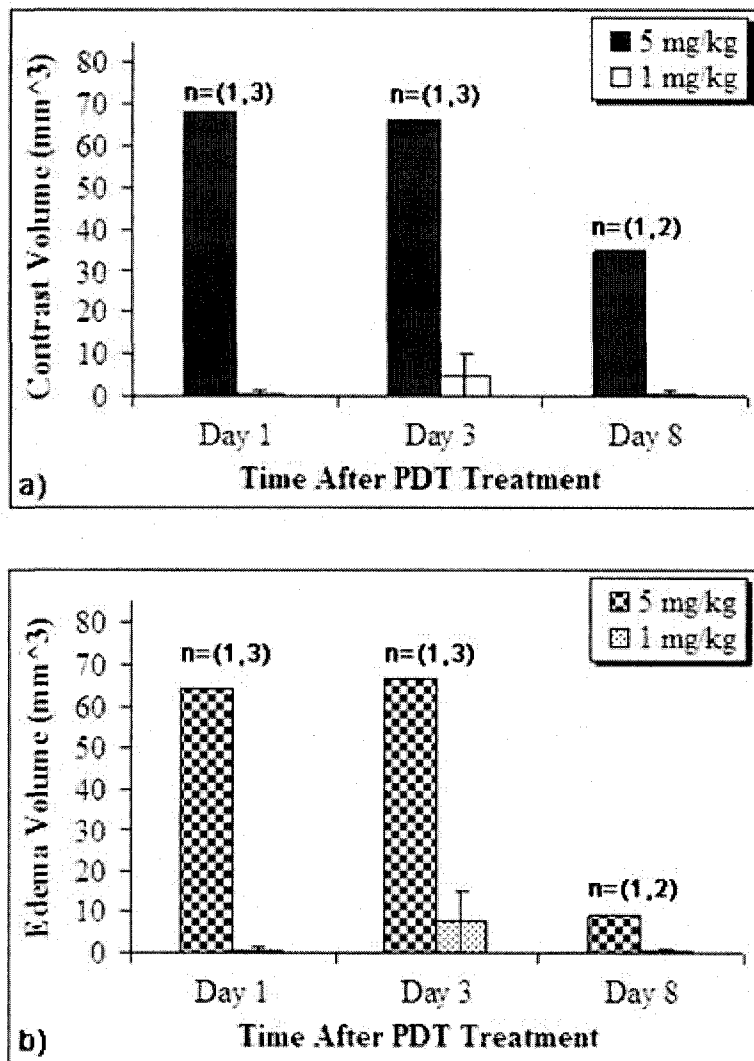


Figure 13. a) Contrast and b) edema volumes induced by PDT with varying photosensitizer concentrations. The animals received 5 or 1 mg/kg (i.p.) of AlPcS_{2a} prior to light treatment (1 J, 10 mW) and were scanned on days 1, 3 and 8 following PDT treatment. The n values listed above each data set indicate the number of animals used to generate the corresponding data bars.

3.4 Effects of Light Fluence Level in AlPcS_{2a}-PDT

Since the lower concentration of AlPcS_{2a} resulted in a smaller amount of BBB disruption, a concentration of 1 mg/kg was used in the rest of the treatments. The effects of light fluence on BBB disruption is illustrated in Figures 14 a and b.

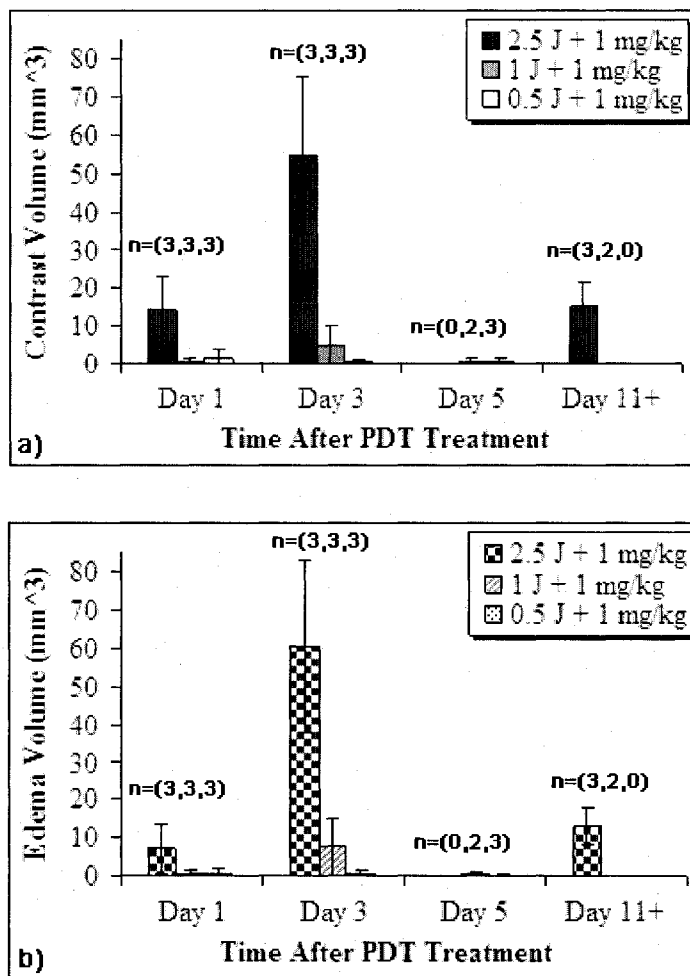


Figure 14. a) Contrast and b) edema volumes induced by PDT with varying light fluence levels. The animals received 1 mg/kg (i.p.) AlPcS_{2a} 48 h prior to light treatment. The n values listed above each data set indicate the number of animals used to generate the corresponding data bars.

As illustrated in Figures 14 a and b, the degree of contrast enhancement and edema formation (and hence BBB disruption) is clearly fluence dependent: the highest light fluence investigated resulted in the greatest edema and contrast enhancement. Only minimal edema and enhancement were observed at the two lower fluences (0.5 and 1 J). Of particular interest is the time evolution of edema and enhancement. In both cases, volumes peaked on day 3 indicating a delay in treatment-induced BBB response. Thereafter, both edema and contrast volumes were observed to decrease. By day 11, only trace amounts of edema and contrast were observed in the 0.5 and 1 J animals, while the high fluence animals still demonstrated significant edema and contrast volumes.

3.5 Surviving Fraction of Rats Following *Clp* Prototoxin Exposure

Figure 15 shows the surviving fraction of rats that received *Clp* prototoxin through either intraperitoneal (i.p.) or intracranial (i.c.) administration at various concentrations. Animals alive after 20 days were considered long-term survivors. As shown in Figure 15, all animals receiving the prototoxin i.c. survived. In contrast, the delivery of *Clp* to animals via intraperitoneal injection proved to be much more toxic resulting in death of all animals receiving a dose of 1:10. It is interesting to note that, although i.p. administration resulted in significant mortality, no evidence of BBB disruption was observed on MR images. Overall, the results suggest that i.c. or i.p. injection of *Clp* at a concentration of 1:100 or lower is well tolerated and therefore provided the rationale for its use in the PCI treatments.

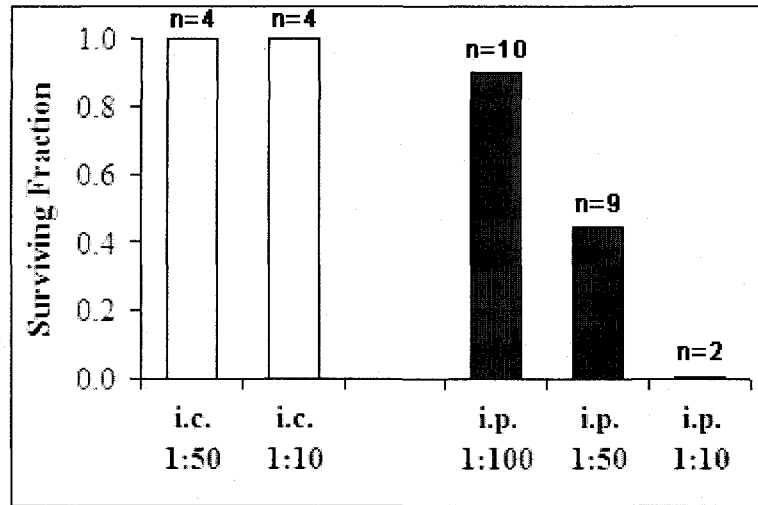


Figure 15. Surviving fraction of animals receiving *Clp* prototoxin through different administration routes at varying concentrations. Two administration methods were compared: i.c. (5 μ l total volume) and i.p. (0.7 ml total volume). The n value above each data bar indicates the total number of animals used per group.

3.6 BBB Disruption Induced by the PCI Effect

The effects of PCI on the BBB for a light fluence of 2.5 J are shown in Figure 16. For comparative purposes, the effects of PDT are also shown. The contrast (Figure 16 a) and edema (Figure 16 b) volumes induced by the two treatment modalities were similar. In both cases, edema and contrast enhancement peaked on the fourth day post-treatment and thereafter rapidly diminished.

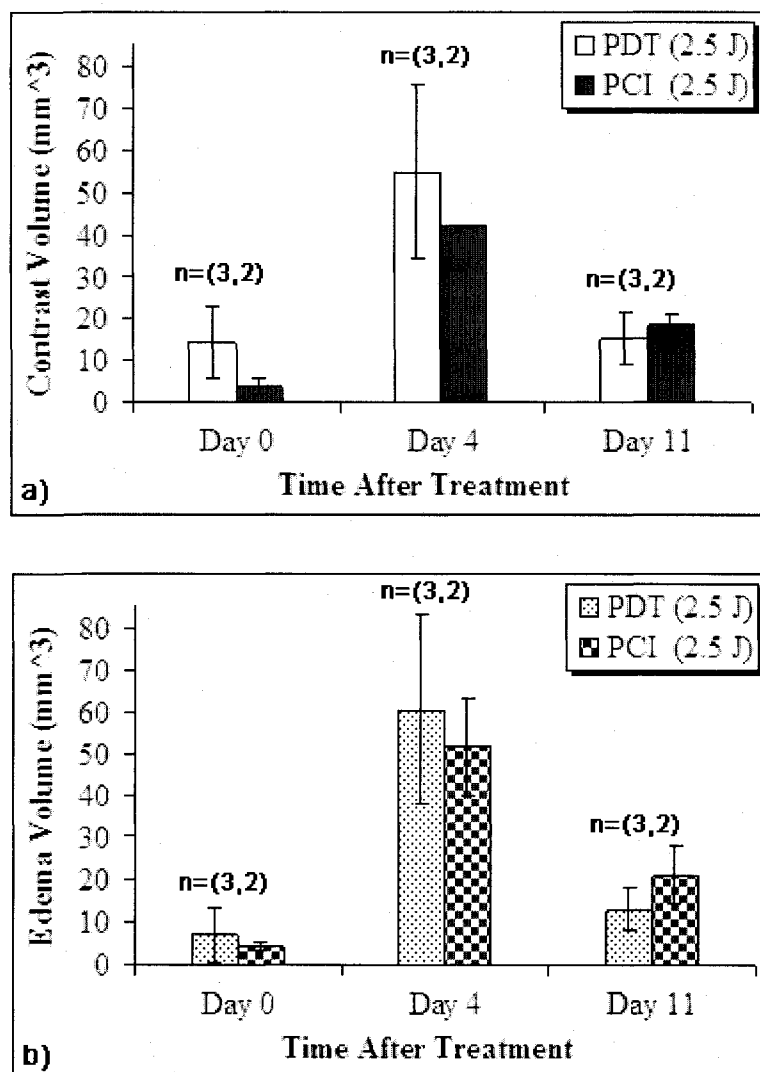


Figure 16. Comparison of a) contrast volume and b) edema volume induced by PDT and PCI at a light fluence of 2.5 J. The animals received 1 mg/kg AlPcS_{2a}. The PCI group of animals also received an i.p. injection of *Clp* at a concentration of 1:50. The n values listed above each data set indicate the number of animals used to generate the corresponding data bars.

The second comparison between PCI and PDT effects on the BBB was performed using a light fluence of 1 J and a *Clp* prototoxin concentration of 1:100 (Figure 17). In

this case, the contrast and edema volumes induced by PCI were significantly greater than those resulting from PDT. A direct comparison of T1-weighted post contrast MRI scans of two animals that received PDT and PCI treatments is shown in Figures 18 a and b, respectively. The images clearly demonstrate the PCI effect on the BBB using this combination of light fluence and prototoxin concentration.

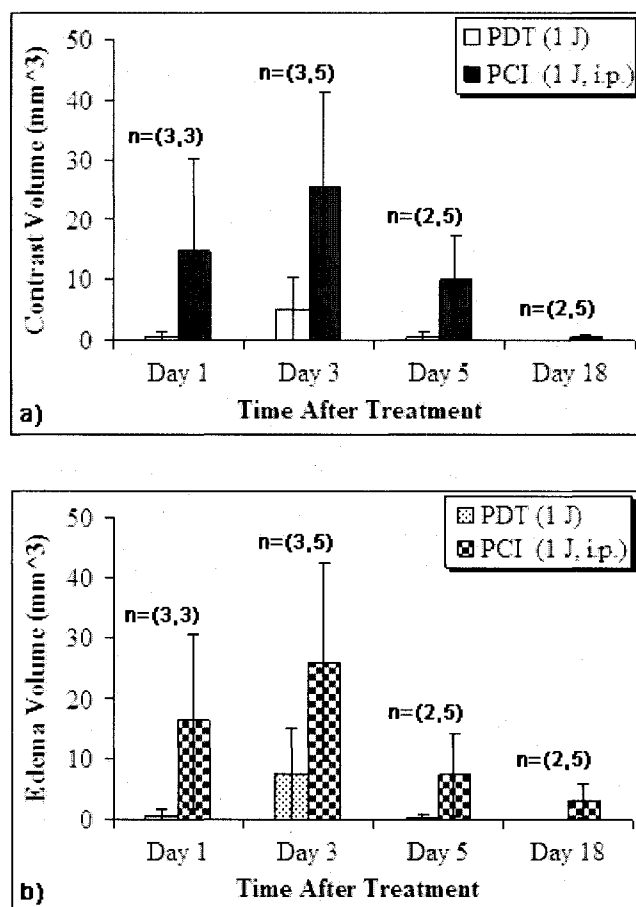


Figure 17. Comparison of a) contrast volume and b) edema volume induced by PDT and PCI (i.p.) at a light fluence of 1 J. The animals received 1 mg/kg ALPcS_{2a}. The PCI group of animals also received an i.p. injection of *Clp* at a concentration of 1:100. The n values listed above each data set indicate the number of animals used to generate the corresponding data bars.

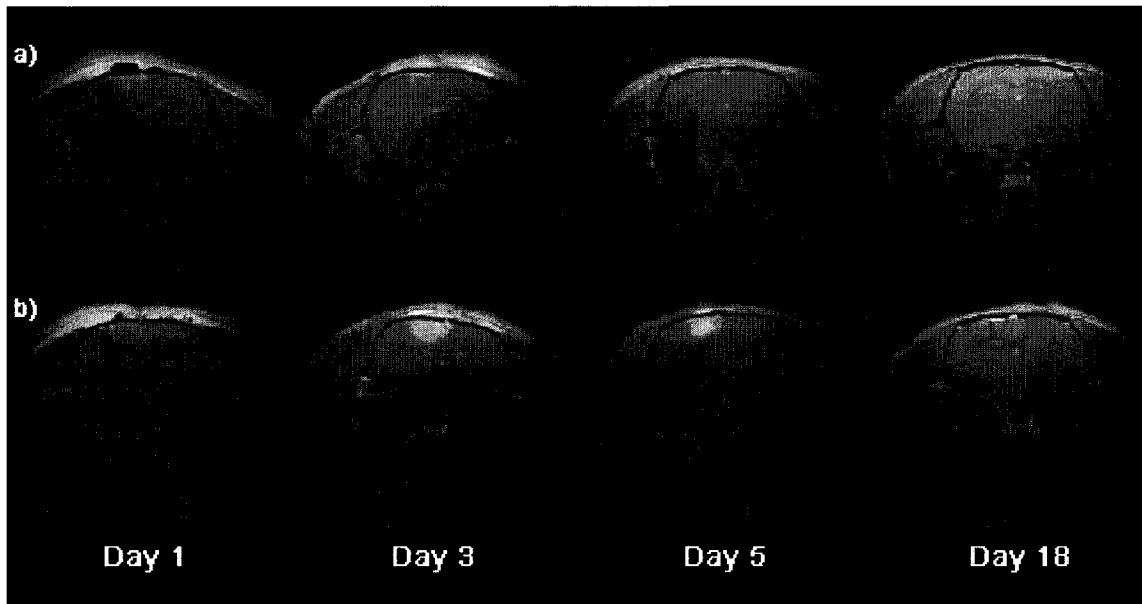


Figure 18. Comparison of T1-weighted post contrast MRI scans after PDT and PCI treatment. a) The PDT treated animal received a light fluence of 1 J; b) the PCI treated animal received a light fluence of 1 J and an i.p. injection of *Clp* at a concentration of 1:100. Both animals were scanned on days 1, 3, 5 and 18 after treatment. All T1 post contrast images were taken 15 minutes following i.p. contrast injection.

The effect of prototoxin administration route was investigated in a series of animals receiving *Clp* prototoxin (1:50) i.c. and subjected to a light fluence of 1 J. As shown in Figure 19, intracranial *Clp* administration produced much lower edema and contrast volumes compared to i.p. administration. In fact, the volumes of both i.c. PCI-induced edema and contrast enhancement were similar to those observed for PDT.

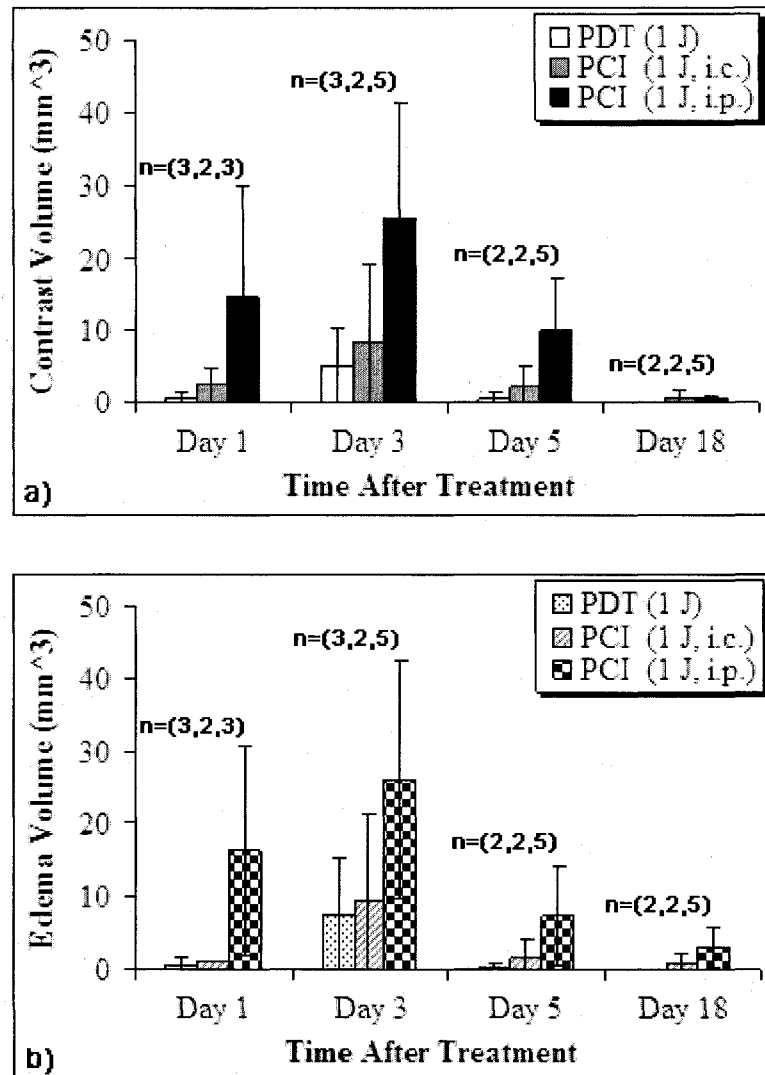


Figure 19. Comparison of a) contrast volume and b) edema volume induced by PDT, PCI (i.c.) and PCI (i.p.) at a light fluence of 1 J. The animals received 1 mg/kg AlPcS_{2a}. The PCI (i.c.) group of animals also received an i.c injection of *Clp* at a concentration of 1:50. The PCI (i.p.) group of animals also received an i.p. injection of *Clp* at a concentration of 1:100. The n values listed above each data set indicate the number of animals used to generate the corresponding data bars.

The last comparison between PCI and PDT effects on the BBB was performed at a light fluence of 0.5 J as shown in Figure 20. Both contrast and edema volumes induced by PDT and PCI at this fluence level were minimal suggesting only a slight degree of BBB disruption.

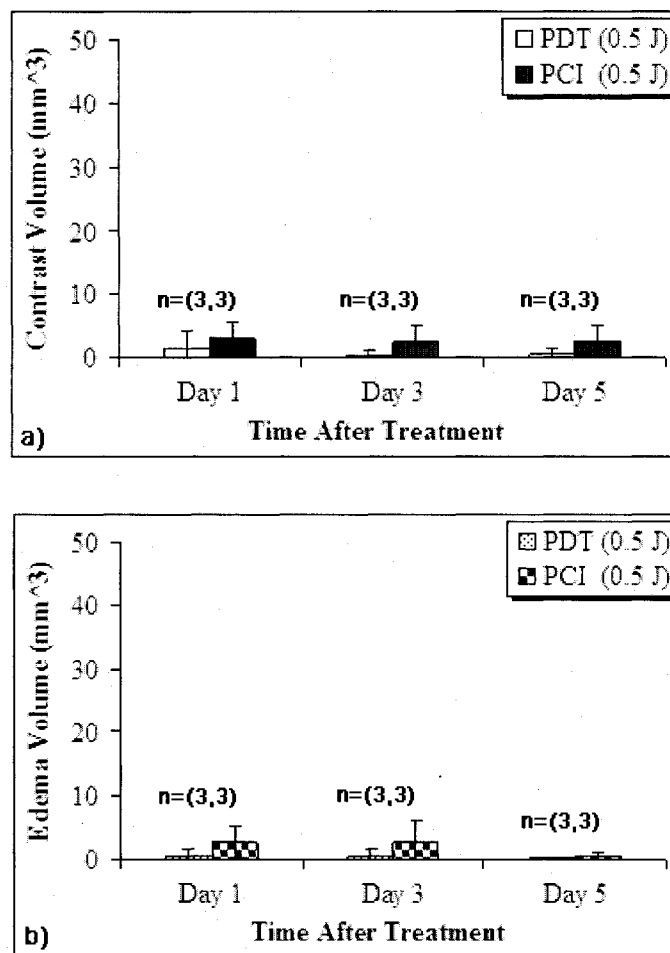


Figure 20. Comparison of a) contrast volume and b) edema volume induced by PDT and PCI at a light fluence of 0.5 J. The animals received 1 mg/kg AlPcS_{2a}. The PCI group of animals also received an i.p. injection of *Clp* at a concentration of 1:100. The n values listed above each data set indicate the number of animals used to generate the corresponding data bars.

CHAPTER 4

DISCUSSION

A previous study has demonstrated that ALA-mediated PDT was highly effective in opening the BBB in a limited region of the normal rat brain (Hirschberg et al., 2008). Results of the present study show that AlPcS_{2a} is a more potent photosensitizer as evidenced by increased mortality (Figure 11) and contrast enhancement (Figure 12) following relatively low light fluences. The increased effectiveness of AlPcS_{2a}-PDT in opening the BBB is most likely due to the site of localization of the photosensitizer. Since AlPcS_{2a} is an amphiphilic molecule it accumulates in cellular membranes such as those of the endothelial cells which constitute the BBB. Therefore, AlPcS_{2a}-PDT causes direct photochemical damage to cell membranes which can lead to disruption of the BBB. In contrast, ALA is a hydrophilic molecule that tends to accumulate in cellular organelles such as the mitochondria. As a result, ALA-PDT is less likely to produce a direct effect on the BBB.

The high mortality observed following interstitial AlPcS_{2a}-PDT is not only due to the preferential localization of AlPcS_{2a} to the BBB, but also due to the light distribution associated with this mode of light delivery. A previous study (Angell-Peterson et al., 2007) demonstrated that the light fluence rate at the tip of an optical fiber inserted directly into the rat brain was 100% higher than the actual power output. A rapid decrease in the interstitial fluence rate was observed with a light penetration depth of about 6 mm

in the rat brain. Surface irradiation was chosen in order to avoid the high fluence rates associated with interstitial light delivery and, as shown in Figure 11, this method of light delivery was well tolerated.

In addition to the light delivery method, the degree of BBB disruption induced by AlPcS_{2a}-PDT was also found to be sensitively dependent on the photosensitizer concentration and light fluence level (Figures 13 and 14). The data show that reductions in AlPcS_{2a} and/or light fluence results in less damage to the BBB.

The data presented in Figure 15 show that the choice of *Cl p* delivery has a profound effect on animal survival. No direct evidence of toxicity to the brain was observed following intracranial injections of relatively high *Cl p* concentrations. Since the distance of drug diffusion through i.c. injection is extremely short, the potential toxicity of *Cl p* is limited to a very small and localized region of the brain, which is not enough to cause any serious effect in the animal even with a relatively high drug concentration. In contrast, the survival of animals administered i.p. injections of *Cl p* was sensitively related to the drug concentration. Since i.p. delivery is systemic, many critical organs (e.g. liver, kidney, intestines, brain) will be exposed to the prototoxin. Therefore, the high mortality rates observed following high doses of *Cl p* (Figure 15) was likely due to massive organ failure. Overall, the results suggest that *Cl p* dilutions of 1:100 can be administered safely in Fischer rats.

Although the risk associated with i.p. delivery is greater than that observed following i.c. administration, i.p. delivery is clearly more effective. The data presented in Figure 19 show that the effects on the BBB, as evidenced by edema and contrast volumes, were similar for PDT and PCI with i.c. delivery of *Cl p*. The ineffectiveness of i.c. delivery is

due to a number of factors. First, the short diffusion distances of macromolecules such as *Cl p* limit treatment volumes to short distances from the injection site. Second, within the prototoxin diffusion volume, only a small fraction of *Cl p* molecules are likely to end up in the brain vasculature and, hence be taken up by the endothelial cells via endocytosis. *Cl p* molecules remaining in the extravascular space have little chance to make it back to the endothelial cells due to the special structure of the BBB.

The data presented in Figure 16 show that both high light fluence (2.5 J) PDT and PCI resulted in significant BBB disruption. Since significant differences between PCI and PDT-induced edema and contrast volumes were not observed, the effects on the BBB were attributed primarily to the PDT effect in the case of both treatments. In contrast, following a light fluence of 1 J, significant differences in both contrast (Figure 17 a) and edema (Figure 17 b) volumes were observed. This was taken to be indicative of a PCI effect. At the lowest light fluence investigated (0.5 J), the data suggest that there was no PCI effect (Figure 20): both PDT and PCI treatments resulted in minimal edema and contrast volumes. Collectively, the data presented in Figures 16, 17 and 20 suggest that the PCI effect is confined to a very narrow range of light fluences and therefore the choice of this parameter is critical for effective PCI.

A likely reason for the failure of high fluence PCI is the generation of high concentrations of singlet oxygen leading to photochemical damage of endosome encapsulated *Cl p*. Conversely, in the case of the low light fluence, the concentration of singlet oxygen generated in the vesicle membrane was likely insufficient to induce serious photochemical damage to this structure thus preventing the release of *Cl p*. In both cases, the biological effects of *Cl p* were compromised thus leading to a significant

diminution of the PCI effect on the BBB. With an optimal light fluence of 1 J, a sufficient level of PDT-induced photochemical damage resulted in the disruption of the vesicle membrane and release of the *Cl p* molecules capable of exerting their toxic effects on the BBB.

PCI is a multi-step procedure and, in addition to light fluence, this therapeutic modality requires exquisite timing for optimal effect. First, the timing between photosensitizer administration and prototoxin delivery is critical: a sufficient amount of AlPcS_{2a} must be present in endothelial cells of the target region prior to *Cl p* injection. If the time interval is too short, the concentration of photosensitizer in the plasma membranes may be insufficient. Similarly, long time intervals may result in the clearance of photosensitizer prior to prototoxin administration. Previous animal studies suggest that a 48 h interval is sufficient. Second, the timing between prototoxin administration and light irradiation is also important. If the interval is too short, the number of endosome-encapsulated *Cl p* molecules will be insufficient for the PCI effect. Conversely, a long time interval increases the likelihood that *Cl p*-laden endosomes will be captured by lysosomes resulting in degradation of the prototoxin. The results of other investigators suggest that time intervals between 1 and 4 h are sufficient.

In comparison with the osmotic opening method of BBB disruption described in section 1.3.3, the biggest advantage of the PCI effect on the BBB is its selectivity. The osmotic opening method involves the administration of a hypertonic solution (e.g. mannitol) to cause shrinkage of the endothelial cells resulting in the disruption of tight junctions and non-selective opening of the BBB. This global disruption of the BBB is problematic because it allows passage of a wide variety of molecules into the brain. Even

though an i.p. injection of *Clp* prototoxin was used in the PCI procedure, and this injection method can lead to a global distribution of prototoxin, the low concentration of prototoxin used (1:100 dilution) was unable to cause BBB damage by itself due to lysosomal degradation of *Clp* molecules trapped in endocytic vesicles. The cytotoxic effect of *Clp* on the BBB is limited to regions of the brain exposed to proper light fluences.

Both PDT and PCI treatments were able to induce a localized BBB disruption in a timely manner. The extent of BBB disruption on different days after PDT or PCI treatment demonstrated a very similar pattern, of which the peak opening appeared to be on day 3 and the disruption was then gradually restored and diminished to the baseline about 18 days after treatment. However, the most important advantage of PCI over PDT is its high efficiency for inducing BBB disruption. As shown in Figures 17 and 18, when using equivalent light fluences of 1 J, the PCI effect induced a much greater extent of BBB disruption than PDT. In other words, in order to achieve similar effects on the BBB, higher light fluences are required for PDT compared to PCI. Unfortunately, higher light fluences increase the potential for edema formation and hence, morbidity and mortality. Therefore, under the appropriate conditions, PCI would appear to be a safe alternative to PDT for selective disruption of the BBB.

The results of the present study suggest that, under the appropriate conditions, PCI is a safe and efficient method for the selective disruption of the BBB in rats. Due to *Clp* toxicity, and the lack of evidence for the existence of specific receptor sites for *Clp* on human brain endothelial membranes, it is highly unlikely that *Clp*-based PCI approaches will be used in human BBB studies. Nevertheless, the results of the present study provide

the basis for further PCI studies using non-toxic vasoactive compounds including bradykinin, leukotrienes and histamine. For example, a number of studies have shown that bradykinin can selectively open the abnormal BBB resulting in an increase in the permeability to both low and high molecular weight neuropharmaceutical agents (Matsukado et al., 1998). Whether these non-toxic agents can be used in the PCI technique to potentiate BBB disruption remains to be shown.

CHAPTER 5

CONCLUSIONS

The PCI effect in normal Fischer rat brain was found to be sensitively dependent on light fluence, photosensitizer concentration, *Cl p* prototoxin concentration and administration route. Selective disruption of the BBB, as determined from MR evaluations of edema and contrast volumes was observed for i.p. administrations of 1:100 stock dilutions of *Cl p* prototoxin and photosensitizer concentrations and light fluences of 1 mg/kg and 1 J respectively. The extent of BBB disruption after PCI treatment increased to its peak level by day 3 and then gradually decreased; the disruption was seen to be restored by day 18.

The aim of future studies will be to improve the PCI method for BBB disruption. First, it is necessary to modify the light delivery method from surface to interstitial irradiation since surface irradiation significantly limits access to various treatment locations due to the short penetration of light in brain tissues. As illustrated in the present work, the main limitation associated with interstitial light delivery is the increased likelihood of edema-induced morbidity and mortality due to high light fluences near the light source. Therefore, additional experiments investigating lower AlPcS_{2a} concentrations, fluence rates and fluences are required in order to optimize interstitial AlPcS_{2a}-PDT. Second, finding a non-toxic agent capable of disrupting the BBB is a requirement for clinical trials.

The ultimate goal of selective and reversible opening of the BBB is to mitigate the passage of anti-cancer drugs across the barrier in order to target infiltrating glioma cells. With this goal in mind, animal studies involving Fischer rats with orthotopic gliomas should be initiated. As a starting point, optimum parameters determined in the present study could be used to selectively disrupt the BBB in rat brains implanted with infiltrating glioma cells. Following administration of a chemotherapeutic agent, animal survival could be compared to non-PCI and chemotherapy-only control animals. In principle, these types of experiments could be extended to evaluate the efficacy of PCI for the treatment of a wide variety of neurological diseases using disease specific therapeutic agents.

REFERENCES

- Abbott N. Physiology of the blood-brain barrier and its consequences for drug transport to the brain. *International Congress Series* 2005; 1277:3-18.
- Abbott N and Romero I. Transporting therapeutics across the blood-brain barrier. *Molecular Medicine Today* 1996; 2:106-113.
- Angell-Peterson E, Hirschberg H and Madsen S. Determination of fluence rate and temperature distributions in the rat brain; implications for photodynamic therapy. *Journal of Biomedical Optics* 2007; 12:014003.
- Athanassiou H, Synodinou M, Maragoudakis E, Paraskevaidis M, Verigos C, Misailidou D, et al. Randomized phase II study of Temozolomide and radiotherapy compared with radiotherapy alone in newly diagnosed GBM. *Journal of Clinical Oncology* 2005; 23:2372-2377.
- Ballabh P, Braun A and Nedergaard M. The blood–brain barrier: an overview: Structure, regulation, and clinical implications. *Neurobiology of Disease* 2004; 16:1-13.
- Berg K, Bommer J and Moan J. Evaluation of sulfonated aluminum phthalocyanines for use in photochemotherapy. Cellular uptake studies. *Cancer Letters* 1989; 44:7-15.
- Berg K, Høgset A, Prasmickaite L, Weyergang A, Bonsted A, Dietze A, Lou P, Bown P, Norum O, Mali H, Møllergård T and Selbo PK. Photochemical internalization (PCI): A novel technology for activation of endocytosed therapeutic agents. *Medical Laser Application* 2006; 21:239-250.
- Berg K, Selbo P, Weyergang A, Dietze A, Prasmickaite L, Bonsted A, Engesaeter B, Angell-Petersen E, Warloe E, Frandsen N and Høgset A. Porphyrin-related photosensitizers for cancer imaging and therapeutic applications. *Journal of Microscopy* 2005; 218:133-147.
- Bhown A and Habeeb A. Structural studies on ϵ -prototoxin of clostridium perfringens type D. localization of the site of tryptic scission necessary for activation to ϵ -toxin. *Biochemical and Biophysical Research Communications* 1977; 78:889-896.
- Buxton D. Use of horseradish peroxidase to study the antagonism of Clostridium welchii (Cl. perfringens) Type D epsilon toxin in mice by the formalinized epsilon prototoxin. *Journal of Comparative Pathology* 1976; 86:67-72.

Calzavara-Pinton P, Venturini M and Sala R. Photodynamic therapy: update 2006 Part 1: Photochemistry and photobiology. *Journal of the European Academy of Dermatology and Venereology* 2007; 21:293-302.

Castano A, Demidova T and Hamblin M. Mechanisms in photodynamic therapy: part one—photosensitizers, photochemistry and cellular localization. *Photodiagnosis and Photodynamic Therapy* 2004; 1:279-293.

Castano A, Demidova T and Hamblin M. Mechanisms in photodynamic therapy: part two—cellular signaling, cell metabolism and modes of cell death. *Photodiagnosis and Photodynamic Therapy* 2005; 2:1-23.

Chamberlain M and Kormanik P. Practical Guidelines for the Treatment of Malignant Gliomas. *West J Med* 1998; 168:114-120.

DeRosa M and Crutchley R. Photosensitized singlet oxygen and its applications. *Coordination Chemistry Reviews* 2002; 233-234:351-371.

Dobrogowska D and Vorbodt A. Quantitative immunocytochemical study of blood–brain barrier glucose transporter (GLUT-1) in four regions of mouse brain. *J Histochem Cytochem* 1999; 47: 1021–1030.

Dorca-Arévalo J, Soler-Jover A, Gibert M, Popoff M, Martín-Satué M and Blasi J. Binding of epsilon-toxin from *Clostridium perfringens* in the nervous system. *Veterinary Microbiology* 2008; 131:14-25.

Finnie J. Neurological disorders produced by *Clostridium perfringens* type D epsilon toxin. *Anaerobe* 2004; 10:145-150.

Finnie J. Ultrastructural changes in the brain of mice given *Clostridium perfringens* type D epsilon toxin. *Journal of Comparative Pathology* 1984a; 94:445-452.

Finnie J. Histopathological changes in the brain of mice given *Clostridium perfringens* type D epsilon toxin. *Journal of Comparative Pathology* 1984b; 94:363-370.

Furnari F, Fenton T, Bachoo R, Mukasa A, Stommel J, Stegh A, Hahn W, Ligon K, Louis D, Brennan C, Chin L, DePinho R and Cavenee W. Malignant astrocytic glioma: genetics, biology, and paths to treatment. *Genes & Development* 2007; 21: 2683-2710.

Gardner D. Pathology of *Clostridium welchii* type D enterotoxaemia: II. Structural and ultrastructural alterations in the tissues of lambs and mice. *Journal of Comparative Pathology* 1973; 83:509-524.

Gloor S, Wachtel M, Bolliger M, Ishihara H, Landmann R and Frei K. Molecular and cellular permeability control at the blood–brain barrier. *Brain Research Reviews* 2001; 36:258-264.

Hirschberg H, Peng Q, Uzal F, Chighvinadze D, **Zhang M** and Madsen S. Disruption of the blood-brain barrier following ALA-mediated photodynamic therapy. *Proceedings of SPIE* 2008; 6842: 68422O1-11.

Huber J, Eggleton R and Davis T. Molecular physiology and pathophysiology of tight junctions in the blood-brain barrier. *Trends in Neurosciences* 2001; 24:719-725.

Høgset A, Prasmickaite L, Selbo P, Hellum M, Engesæter B, Bonsted A and Berg K. Photochemical internalisation in drug and gene delivery. *Advanced Drug Delivery Reviews* 2004; 56:95-115.

Kemper E, Boogerd W, Thuis I, Beijnen J and Telling O. Modulation of the blood-brain barrier in oncology: therapeutic opportunities for the treatment of brain tumours. *Cancer Treatment Reviews* 2004; 30:425-423.

Liu R, Chang S, Prados M. Recent advances in the treatment of central nervous system tumors. *Update on Cancer Therapeutics* 2008; 3:49-79.

Louis D. Molecular Pathology of Malignant Gliomas. *Annu. Rev. Pathol. Mech. Dis.* 2006; 1:97-117.

Maman N, Dhami S, Phillips D and Brault D. Kinetic and equilibrium studies of incorporation of di-sulfonated aluminum phthalocyanine into unilamellar vesicles. *Biochimica et Biophysica Acta (BBA) - Biomembranes* 1999; 1420:168-178.

Martini F. *Fundamentals of anatomy & physiology*. 7th edition. Boston: Pearson Custom Publishing. 2006.

Matsukado K, Sugita M and Black K. Intracarotid low dose bradykinin infusion selectively increases tumor permeability through activation of bradykinin B2 receptors in malignant gliomas. *Brain Research* 1998; 792:10-15.

Matter K and Balda M. Signalling to and from tight junctions. *Nature Reviews Molecular Cell Biology* 2003; 4:225-236.

Morgan K and Kelly B. Ultrastructural study of brain lesions produced in mice by the administration of *Clostridium welchii* type D epsilon toxin. *Journal of Comparative Pathology* 1974; 84:181-191.

Morgan K, Kelly B and Buxton D. Vascular leakage produced in the brains of mice by *Clostridium welchii* type D toxin. *Journal of Comparative Pathology* 1975; 85:461-466.

Nagahama M and Sakurai J. Distribution of labeled *Clostridium perfringens* epsilon toxin in mice. *Toxicon* 1991; 29:211-217.

Neuwelt E, Williams P, Mickwyb B, Frenkeib E and Hennera D. Therapeutic Dilemma of Disseminated CNS Germoma and the Potential of Increased Platinum-Based Chemotherapy Delivery with Osmotic Blood-Brain Barrier Disruption. *Pediatr Neurosurg* 1994; 21:16-22.

Paquette B, Ali H, Langlois R and Van Lier J. Biological activities of phthalocyanines - VIII. Cellular distribution in V-79 Chinese Hamster cells and phototoxicity of selectively sulfonated aluminum phthalocyanines. *Photochem. Photobiol.* 1988; 47:215-220.

Pardridge W. The Blood-Brain Barrier: Bottleneck in Brain Drug Development. *NeuroRX* 2005; 2:3-14;

Plaetzer K, Krammer B, Berlanda J, Berr F and Kiesslich T. Photophysics and photochemistry of photodynamic therapy: fundamental aspects. *Lasers in Medical Science* 2008; doi: 10.1007/s10103-008-0539-1.

Prasmickaite L, Høgset A, Selbo P, Engesæter B, Hellum M and Berg K. Photochemical disruption of endocytic vesicles before delivery of drugs: a new strategy for cancer therapy. *British Journal of Cancer* 2002; 86:652-657.

Sakurai J. Toxins of *Clostridium perfringens*. *Reviews in Medical Microbiology* 1995; 6:175-185.

Scherrmann J. Drug delivery to brain via the blood-brain barrier. *Vascular Pharmacology* 2002; 38:349-354.

Soler-Jover A, Dorca J, Popoff M, Gibert M, Saura J, Tusell J, Serratosa J, Blasi J and Martín-Satué M. Distribution of *Clostridium perfringens* epsilon toxin in the brains of acutely intoxicated mice and its effect upon glial cells. *Toxicon* 2007; 50:530-540.

Stupp R, Mason W, van den Bent M, Weller M, Fisher B, Taphoorn M, Belanger K, Brandes A, Marosi C, Bogdahn U, Curschmann J, Janzer R, Ludwin S, Gorlia T, Allgeier A, Lacombe D, Cairncross J, Eisenhauer E and Mirimanoff R. Radiotherapy plus Concomitant and Adjuvant Temozolomide for Glioblastoma. *New England Journal of Medicine* 2005; 352:987-996.

Wolburg H and Lippoldt A. Tight junctions of the blood-brain barrier: development, composition and regulation. *Vascular Pharmacology* 2002; 38:323-337.

Worthington R and Mulders M. The effect of *Clostridium perfringens* epsilon toxin on the blood brain barrier of mice. *Onderstepoort Journal of Veterinary Research* 1975; 42:25-28.

Zhu C, Ghabriel M, Blumbergs P, Reilly P, Manavis J, Youssef J, Hatami S and Finnie J. *Clostridium perfringens* Prototoxin-Induced Alteration of Endothelial Barrier Antigen

(EBA) Immunoreactivity at the Blood–Brain Barrier (BBB). *Experimental Neurology* 2001; 169:72–82.

VITA

Graduate College
University of Nevada, Las Vegas

Michelle Jie Zhang

Home Address:

4356 Greenhill Drive
Las Vegas, Nevada 89121

Degrees:

Bachelor of Arts, Computer Science, 2004
University of Nevada, Las Vegas

Special Honors and Awards:

Magna Cum Laude

Publications:

Hirschberg H, Peng Q, Uzal F, Chighvinadze D, **Zhang M** and Madsen S. Disruption of the blood-brain barrier following ALA-mediated photodynamic therapy. Proceedings of SPIE 2008; 6842:68422O1-11.

Hirschberg H, Uzal F, Chighvinadze D, **Zhang M**, Peng Q and Madsen S. Disruption of the blood brain barrier following ALA-mediated photodynamic therapy. Lasers in Surgery and Medicine 2008.

Thesis Title: Selective Disruption of the Blood-Brain Barrier by Photochemical Internalization

Thesis Examination Committee:

Committee Chair, Dr. Steen Madsen, Ph.D.
Committee Member, Dr. Phillip Patton, Ph.D.
Committee Member, Dr. Ralf Sudowe, Ph.D.
Committee Member, Dr. Henry Hirschberg, M.D., Ph.D.
Graduate College Representative, Dr. Daniel Young, PT, DPT.